

Inclusive processes

10.1 Introduction

Though many-body final states provide the bulk of the high energy scattering cross-section, individual final states are hard to analyse. They are hard to extract experimentally because it is essential to test (using energy, momentum, and quantum-number arguments) that the final-state particles observed in the detecting apparatus were the only particles produced, and to exclude all the many other different types of events which could have occurred. In particular the production of neutral particles is especially hard to detect. And, as we have found in the previous chapter, final states are also hard to analyse theoretically both because the number of independent variables increases rapidly with the number of particles, and because only a fraction of the events occur in regions of phase space which are easy to parametrize, such as the low sub-energy resonance region, or the high sub-energy Regge region.

Because of these problems it has been found more useful to concentrate attention on so-called ‘inclusive processes’, that is, processes in which a given particle or set of particles is found to occur in the final state, but no questions are asked about all the other particles which may also be present in this final state. Thus we have the single-particle inclusive cross-section for the process

$$1 + 2 \rightarrow 3 + X \quad (10.1.1)$$

(fig. 10.1 (a)) where 3 is a specified type of particle (for example it may be specifically a π^- , or more generally any negatively charged particle), and X includes all the particles which may be produced with 3, given the need to conserve energy, momentum and quantum numbers. Obviously we must have, to conserve four-momentum and charge,

$$p_X = p_1 + p_2 - p_3, \quad Q_X = Q_1 + Q_2 - Q_3 \quad (10.1.2)$$

etc. Similarly, the two-particle inclusive process is

$$1 + 2 \rightarrow 3 + 4 + X \quad (10.1.3)$$

where 3 and 4 are specified types of particles, and X is anything (fig. 10.1 (b)).

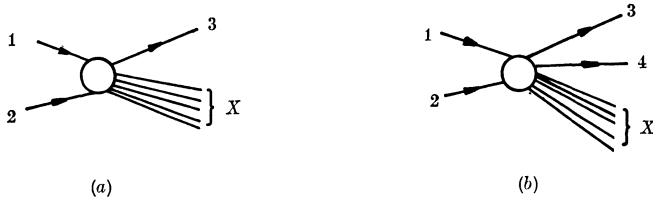


FIG. 10.1 (a) The single-particle inclusive process $1 + 2 \rightarrow 3 + X$.
 (b) The two-particle inclusive process $1 + 2 \rightarrow 3 + 4 + X$.

Such processes are fairly easy to identify experimentally since all one has to do is to verify that a particle (or particles) of the specified type(s) has been detected. It is necessary to measure the momentum only of the detected particle(s) (in addition to the beam momentum) to determine the event completely, because, for the process (10.1.1) for example, there are only three independent variables (s_{12} , t_{13} and M_X), as we shall see in the next section.

Also, through a rather ingenious generalization of the optical theorem, due to Mueller, it is surprisingly simple to obtain Regge predictions about the high energy behaviour of such processes. So in recent years a great deal more progress has been made in understanding many-body processes through this inclusive approach than by analysing particular exclusive final states such as $1 + 2 \rightarrow 3 + 4 + 5$.

This chapter is devoted to the Regge analysis of inclusive processes. We begin by discussing their kinematics, and the definition of an inclusive cross-section, before introducing Mueller's theorem which is then used to make a variety of Regge predictions. Useful reviews of this subject have been made by Horn (1972), Frazer *et al.* (1972) and Morrison (1972).

10.2 The kinematics of inclusive processes

We consider the process (10.1.1) shown in fig. 10.1(a). As usual we work in the s -channel centre-of-mass system in which the four-momenta are

$$\left. \begin{aligned} p_1 &= (E_1, 0, 0, p_z), & p_1^2 &= E_1^2 - p_z^2 = m_1^2 \\ p_2 &= (E_2, 0, 0, -p_z), & p_2^2 &= E_2^2 - p_z^2 = m_2^2 \\ p_3 &= (E_3, \mathbf{p}_{3T}, p_{3L}), & p_3^2 &= E_3^2 - \mathbf{p}_{3T}^2 - p_{3L}^2 = m_3^2 \end{aligned} \right\} \quad (10.2.1)$$

The z axis is defined as the direction of motion of particle 1, and (as in fig. 10.2) we have resolved the momentum of 3 into its longi-

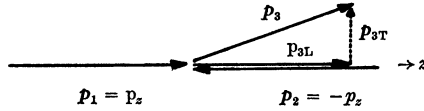


FIG. 10.2 Momenta in $1 + 2 \rightarrow 3 + X$: $p_1 = p_z$, $p_2 = -p_z$, both along the z axis, and p_3 has been resolved into components p_{3L} along the z axis, and p_{3T} transverse to it.

tudinal component, p_{3L} , along this z axis, and its components transverse to this axis which are represented by the two-component vector p_{3T} . This distinction is very useful because it is found experimentally that though at high energy p_{3L} may take on almost any kinematically allowed value, from $p_{3L} \approx p_z$ if 3 is produced as a fragment of particle 1, to $p_{3L} \approx -p_z$ if it is produced from 2, the transverse component is usually rather small, very few events having $|p_{3T}| > 0.5 \text{ GeV}/c$. In fact $\langle p_{3T} \rangle \approx 0.3\text{--}0.4 \text{ GeV}/c$ whatever the beam energy.

Usually the majority of the particles in the final state are pions, presumably because the pion is the lightest hadron, with much smaller numbers of kaons, baryons etc., so typically $m_3 \lesssim 1 \text{ GeV}/c^2$. It is convenient to introduce the ‘longitudinal mass’ μ_3 defined by

$$\mu_3 \equiv (m_3^2 + p_{3T}^2)^{\frac{1}{2}} \tag{10.2.2}$$

which is also generally $\leq 1 \text{ GeV}/c^2$, so that, from (10.2.1), μ_3 gives the effective mass associated with the longitudinal momentum, i.e.

$$E_3^2 = \mu_3^2 + p_{3L}^2 \tag{10.2.3}$$

As usual $s = s_{12} \equiv (p_1 + p_2)^2$, so that E_1 and E_2 are given by (1.7.8) and (1.7.9), and $p_z = q_{s12}$ is given by (1.7.10), and so

$$p_z^2 \xrightarrow{s \rightarrow \infty} \frac{s}{4}, \quad E_1, E_2 \xrightarrow{s \rightarrow \infty} \frac{\sqrt{s}}{2} \quad \text{for } s \gg m_1^2, m_2^2 \tag{10.2.4}$$

For the final state $s = (p_3 + p_X)^2$ and we define the ‘missing mass’ by

$$M^2 \equiv M_X^2 \equiv (p_1 + p_2 - p_3)^2 = s + m_3^2 - 2E_3\sqrt{s} \tag{10.2.6}$$

from (10.2.1) with (1.7.5). Obviously M takes the place of m_4 in the expressions (1.7.9) and (1.7.12) for the final-state energy and momentum, so

$$p_3^2 = p_{3T}^2 + p_{3L}^2 = \frac{1}{4s} [s - (m_3 + M)^2] [s - (m_3 - M)^2]$$

$$\xrightarrow{s, M^2 \rightarrow \infty} \frac{(s - M^2)^2}{4s} \xrightarrow{s \gg M^2} \frac{s}{4} \tag{10.2.7}$$

$$E_3 = \frac{1}{2\sqrt{s}} (s + m_3^2 - M^2) \xrightarrow{s, M^2 \rightarrow \infty} \frac{s - M^2}{2\sqrt{s}} \xrightarrow{s \gg M^2} \frac{\sqrt{s}}{2} \tag{10.2.8}$$

Since p_{3T}^2 is small $p_{3L}^2 \approx p_3^2 \rightarrow \frac{(s - M^2)^2}{4s}$

and so
$$\frac{M^2}{s} \approx 1 - \frac{2p_{3L}}{\sqrt{s}} \tag{10.2.9}$$

Another independent variable is

$$t_{13} = t \equiv (p_1 - p_3)^2 = m_1^2 + m_3^2 - 2p_1 \cdot p_3 = m_1^2 + m_3^2 - 2E_1 E_3 + 2p_2 p_{3L}$$

$$\xrightarrow{s \rightarrow \infty} -\sqrt{s}(E_3 - p_{3L}) = -\sqrt{s} \frac{E_3^2 - p_{3L}^2}{E_3 + p_{3L}} = -\frac{s\mu_3^2}{s - M^2} \tag{10.2.10}$$

using (10.2.4), followed by (10.2.3), (10.2.7) and (10.2.8). Similarly

$$u \equiv (p_2 - p_3)^2 \rightarrow -s(E_3 + p_{3L}) \tag{10.2.11}$$

and like (1.7.18)
$$\frac{1}{2}s + t + u = m_1^2 + m_2^2 + m_3^2 + M^2 \tag{10.2.12}$$

So s , t and M^2 form a complete set of variables from which all the other kinematical quantities can readily be obtained.

However, two other variables are also frequently used. One of these is the Feynman variable, or ‘reduced longitudinal momentum’ x , defined by (Feynman 1969)

$$x_3 \equiv \frac{p_{3L}}{p_{3L \max}} \tag{10.2.13}$$

Now from (10.2.9) the maximum value of p_{3L} occurs when $M^2 \rightarrow 0$ so

$$x_3 \approx \frac{2p_{3L}}{\sqrt{s}} \quad \text{or} \quad x_3 \approx 1 - \frac{M^2}{s} \tag{10.2.14}$$

(though in fact M_{\min}^2 is the mass of the lightest particle which can be produced, and is > 0).

Sometimes (10.2.14) is used to define x instead of (10.2.13), but the equations are equivalent only to the extent that $m_{1,2,3}$ and $|p_{3T}|$ can be neglected compared with s and M^2 . Clearly $x_1 = 1$ and $x_2 = -1$, and if $x_3 \approx 1$ it means that 3 has acquired most of the momentum of 1 and we can say that 3 is a ‘fragment’ of 1, or if $x \approx -1$, 3 is a fragment of 2 (see fig. 10.3). The ‘central region’ $x_3 \approx 0$ implies that 3 is approximately stationary in the centre-of-mass system and so is not directly connected with 1 or 2. These ideas will be made a bit more precise below. From (10.2.10) and (10.2.14) we have

$$t \rightarrow -\frac{\mu_3^2}{1 - x_3} \tag{10.2.15}$$

so that s , x_3 and p_{3T}^2 provide a complete set of variables.

The other commonly employed variable is the rapidity y , defined by (de Tar 1971)

$$y_3 \equiv \frac{1}{2} \log \left(\frac{E_3 + p_{3L}}{E_3 - p_{3L}} \right) \tag{10.2.16}$$

from which we obtain, using (10.2.3),

$$\sinh y_3 = \frac{p_{3L}}{\mu_3}, \quad \cosh y_3 = \frac{E_3}{\mu_3} \tag{10.2.17}$$

and so the components of p_3 are

$$p_3 = (\mu_3 \cosh y_3, \mathbf{p}_{3T}, \mu_3 \sinh y_3) \tag{10.2.18}$$

This variable has the advantage that under a Lorentz boost by velocity v along the z axis (we use $c \equiv 1$ so $\beta \equiv v$, $\gamma \equiv (1 - v^2)^{-\frac{1}{2}}$ in the usual notation)

$$p_3 = (E_3, \mathbf{p}_{3T}, p_{3L}) \xrightarrow{\text{Lorentz transformation}} (\gamma(E_3 + vp_{3L}), \mathbf{p}_{3T}, \gamma(p_{3L} + vE_3)) \tag{10.2.19}$$

and if these transformed values are substituted into (10.2.16)

$$y_3 \xrightarrow{\text{Lorentz transformation}} y_3 + \frac{1}{2} \log \left(\frac{1+v}{1-v} \right) \tag{10.2.20}$$

So the rapidity has very simple transformation properties along the beam axis. In fact a particle of rest mass m moving along the z axis with velocity v has $E = \gamma m$, $p_L = \gamma mv$ and hence

$$y = \frac{1}{2} \log \left(\frac{1+v}{1-v} \right) \xrightarrow{v \ll 1} v$$

so in the non-relativistic limit, $v \ll c \equiv 1$, rapidity \rightarrow velocity (which accounts for the name). But, unlike velocities, rapidities simply add like (10.2.20), even relativistically.

In the centre-of-mass system

$$\begin{aligned} y_1 &= \frac{1}{2} \log \left(\frac{E_1 + p_z}{E_1 - p_z} \right) = \frac{1}{2} \log \left(\frac{(E_1 + p_z)^2}{E_1^2 - p_z^2} \right) \\ &= \frac{1}{2} \log \left(\frac{(E_1 + p_z)^2}{m_1^2} \right) \xrightarrow{s \rightarrow \infty} \frac{1}{2} \log \left(\frac{s}{m_1^2} \right) \end{aligned} \tag{10.2.21}$$

using (10.2.1) and (10.2.4), and likewise $y_2 \rightarrow \frac{1}{2} \log (m_2^2/s)$

$$\text{so} \quad y_1 - y_2 \rightarrow \log \frac{s}{m_1 m_2}, \quad \text{or} \quad s \rightarrow m_1 m_2 e^{(y_1 - y_2)} \tag{10.2.22}$$

Also, from (10.2.15) and (10.2.2), in the centre-of-mass system,

$$y_3 = \frac{1}{2} \log \left(\frac{(E_3 + p_{3L})^2}{\mu_3^2} \right) \tag{10.2.23}$$

and since, from (10.2.8) and (10.2.7), the extreme values (which occur when $M^2 \rightarrow 0$) are $E_3 \approx \sqrt{s}/2$, $p_{3L} \approx \pm \sqrt{s}/2$, we find

$$y_{3 \max} = \frac{1}{2} \log \left(\frac{s}{\mu_3^2} \right), \quad y_{3 \min} = -\frac{1}{2} \log \left(\frac{s}{\mu_3^2} \right) \tag{10.2.24}$$

so the range of y_3 is

$$Y_3 \equiv y_{3 \max} - y_{3 \min} = \log \left(\frac{s}{\mu_3^2} \right) \tag{10.2.25}$$

The maximum occurs when 3 takes on the longitudinal momentum of 1, and the minimum when it takes on that of 2, as in figs. 10.3 (a), (b), while $y_3 = 0$ corresponds to 3 being at rest in the centre-of-mass system. It is sometimes convenient to introduce the reduced rapidity

$$\tilde{y}_3 \equiv \frac{2y_3}{Y_3} \tag{10.2.26}$$

which like x_3 has the range $-1 \leq \tilde{y}_3 \leq 1$. However, \tilde{y}_3 and x_3 are not identical except at the three points $-1, 0, +1$, since as $s \rightarrow \infty$ all particles whose $|p_{3L}| \rightarrow \infty$ move towards $x = 0$. A boost to the laboratory frame (particle 2 at rest) is just, from (10.2.20),

$$y_3 \rightarrow y_3 + \frac{1}{2} \log \left(\frac{s}{\mu_3^2} \right) \tag{10.2.27}$$

as shown in fig. 10.4 (a). From (10.2.10) and (10.2.11) y_3 is related to s, t, u and M^2 by

$$y_3 \rightarrow \frac{1}{2} \log \left(\frac{u}{t} \right) \rightarrow \log \left(\frac{M^2 - s - t}{t} \right) \tag{10.2.28}$$

The quantities $s, y_3, \mathbf{p}_{3T}^2$ thus provide another complete set of variables for the single-particle inclusive process.

10.3 Inclusive cross-sections

In (1.8.5) we wrote down an expression for the cross-section $\sigma_{12 \rightarrow n}$, giving the probability per unit incident flux of n particles being produced in the final state; and in (1.8.7) we summed these to obtain the total cross-section $\sigma_{12}^{\text{tot}} \equiv \sigma_{12 \rightarrow \text{all}}$. Correspondingly the cross-section

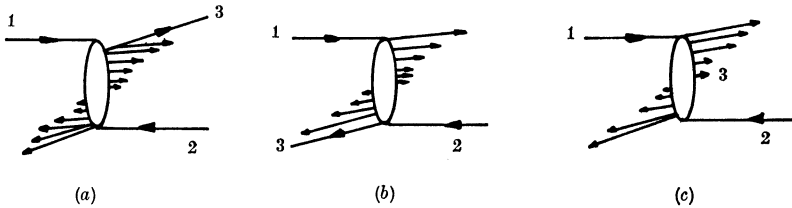


FIG. 10.3 Particle 3 produced (a) as a fragment of 1, (b) as a fragment of 2, and (c) in the central region where it is not associated directly with either incoming particle.

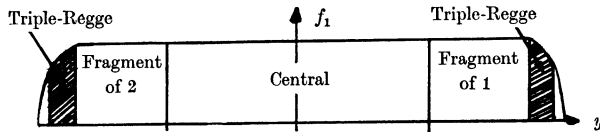
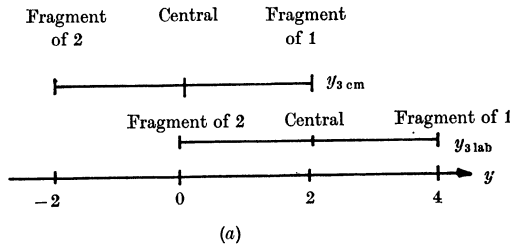


FIG. 10.4 (a) Transformation from laboratory-frame (2 at rest) to centre-of-mass frames rapidities for $Y = 4$; y_{cm} is simply displaced from y_{lab} by 2 units. (b) The different regions of the rapidity plot to be discussed below.

for producing at least one particle of type 3 plus anything is given by

$$\sigma_{12 \rightarrow 3X} = \frac{1}{4q_s \sqrt{s}} \sum_{n=0}^{\infty} \sum_{n_3=1}^{\infty} \int d\Phi_{n+n_3} |\langle p'_1 \dots p'_n, p_3^1 \dots p_3^{n_3} | A | p_1 p_2 \rangle|^2 \tag{10.3.1}$$

where the $p_3^l, l = 1, \dots, n_3$, are the momenta of the n_3 particles of type 3 in the final state, and p'_1, \dots, p'_n are the momenta of the n other particles which also appear ($n + n_3 \geq 2$). So the probability per unit incident flux of detecting a particle of type 3 within the phase-space volume element d^3p_3 (i.e. within the element of solid angle $d\Omega$, with momentum between p_3 and $p_3 + dp_3$) is given by (cf. (1.8.17))

$$\frac{d^3\sigma}{d^3p_3} = \frac{1}{4q_s \sqrt{s}} \sum_{n=0}^{\infty} \sum_{n_3=1}^{\infty} \int d\Phi_{n+n_3} \sum_{l=1}^{n_3} \delta^3(\mathbf{p}_3 - \mathbf{p}_3^l) |\langle A \rangle|^2 \tag{10.3.2}$$

where we have summed over all the n_3 particles of type 3 in the final state. However, this cross-section is frame-dependent, and instead it is preferable to use the invariance of $d^3\mathbf{p}/2E(2\pi)^3$ (shown in (1.2.7)) to define the invariant single-particle distribution by

$$f_1^{12 \rightarrow 3X}(\mathbf{p}_3, s) \equiv 16\pi^3 E_3 \frac{d^3\sigma}{d^3\mathbf{p}_3} \tag{10.3.3}$$

This may also be expressed in terms of our other variables. For example, using $d^3\mathbf{p}_3 = \pi |\mathbf{p}_3| d|\mathbf{p}_3|^2 d(\cos \theta)$ with (10.2.10) and (10.2.7) we obtain

$$f_1 = 16\pi^3 \frac{2p_z \sqrt{s}}{\pi} \frac{d^2\sigma}{dt dM^2} \xrightarrow{s \rightarrow \infty} 16\pi^2 s \frac{d^2\sigma}{dt dM^2} \tag{10.3.4}$$

or, writing $d^3\mathbf{p}_3 = \pi d\mathbf{p}_{3T}^2 dp_{3L}$ and noting that, from (10.2.18),

$$\frac{dp_{3L}}{dy_3} = \mu_3 \frac{d \sinh y_3}{dy_3} = \mu_3 \cosh y_3 = E_3$$

we get
$$f_1 = 16\pi^2 \frac{d^2\sigma}{d(\mathbf{p}_{3T}^2) dy} \tag{10.3.5}$$

Or since from (10.2.14), (10.2.17) and (10.2.3)

$$\frac{dx_3}{dy_3} = \frac{2\mu_3}{\sqrt{s}} \cosh y_3 = \frac{2E_3}{\sqrt{s}} = \left(x_3^2 + \frac{4\mu_3^2}{s}\right)^{\frac{1}{2}}$$

we find

$$f_1 = 16\pi^2 \left(x^2 + \frac{4\mu_3^2}{s}\right)^{\frac{1}{2}} \frac{d^2\sigma}{dx d(\mathbf{p}_{3T}^2)} \xrightarrow{s \rightarrow \infty} 16\pi^2 x_3 \frac{d^2\sigma}{dx_3 d(\mathbf{p}_{3T}^2)} \tag{10.3.6}$$

All of the expressions (10.3.3)–(10.3.6) are used in the literature.

The total single-particle inclusive cross-section is

$$\int f_1(\mathbf{p}_3, s) \frac{d^3\mathbf{p}_3}{16\pi^3 E_3} = \frac{1}{4q_s \sqrt{s}} \sum_{n+n_3=2}^{\infty} \int d\Phi_{n+n_3} \sum_{l=1}^{n_3} \times \int d^3\mathbf{p}_3 \delta^3(\mathbf{p}_3 - \mathbf{p}_3^l) | \langle A | \rangle|^2 = \sum_{n_3=1}^{\infty} n_3 \sigma(1+2 \rightarrow n_3 + X') \tag{10.3.7}$$

where $\sigma(1+2 \rightarrow n_3 + X')$ is the total cross-section for producing n_3 particles of type 3, plus X' , which represents everything else produced but includes no particles of type 3. (So σ is given by (10.3.1) summed over n but not over n_3 .) The weighting by n_3 occurs because of the extra summation over l in (10.3.2). So if we define the average multiplicity of particles of type 3 by

$$\langle n_3 \rangle = \frac{\sum_{n_3=0}^{\infty} n_3 \sigma(1+2 \rightarrow n_3 + X')}{\sum_{n_3=0}^{\infty} \sigma(1+2 \rightarrow n_3 + X')} = \frac{\sum_{n_3=0}^{\infty} n_3 \sigma(1+2 \rightarrow n_3 + X')}{\sigma_{12 \rightarrow \text{all}}^{\text{tot}}} \tag{10.3.8}$$

then
$$\int f_1(\mathbf{p}_3, s) \frac{d^3\mathbf{p}_3}{16\pi^3 E_3} = \langle n_3 \rangle \sigma_{12}^{\text{tot}} \tag{10.3.9}$$

so the total inclusive cross-section is the total cross-section weighted by the average multiplicity. The physical reason for this weighting is, of course, that if the detecting apparatus is set up to register an event every time a particle of type 3 enters then those events in which two particles of type 3 occur will be counted twice, and so on. This multiple counting gives inclusive cross-sections many of their special properties.

It is sometimes convenient to introduce

$$\rho_1(\mathbf{p}_3, s) \equiv \frac{f_1(\mathbf{p}_3, s)}{\sigma_{12}^{\text{tot}}(s)} \tag{10.3.10}$$

so that
$$F_1(s) \equiv \int \rho_1(\mathbf{p}_3, s) \frac{d^3\mathbf{p}_3}{16\pi^3 E_3} = \langle n_3(s) \rangle \tag{10.3.11}$$

Empirically it is found (fig. 10.5) that for large $\langle n_3 \rangle$ and s

$$\langle n_3(s) \rangle \approx A + B \log s$$

which, since $\sigma_{12}^{\text{tot}} \approx \text{constant}$, means that $\int f_1 d^3\mathbf{p}_3 / 16\pi^3 E_3$ is increasing like $\log s$. So as the collision energy increases only a decreasing fraction of it is used to produce new particles, the rest being taken up by the kinetic energy of the final-state particles. We shall see below how this can be explained.

Likewise, we can define the two-particle inclusive distribution, giving the probability per unit flux of producing, in the process $1 + 2 \rightarrow 3 + 4 + X$, a particle of type 3 in $d^3\mathbf{p}_3$ and a particle of type 4 in $d^3\mathbf{p}_4$, by

$$\begin{aligned} f_2(\mathbf{p}_3, \mathbf{p}_4, s) &\equiv 4(2\pi)^6 E_3 E_4 \frac{d^3\sigma}{d^3\mathbf{p}_3 d^3\mathbf{p}_4} \\ &= \frac{1}{4q_s \sqrt{s}} \sum_{n=0}^{\infty} \sum_{n_3=1}^{\infty} \sum_{n_4=1}^{\infty} d\Phi_{n+n_3+n_4} \sum_{l=1}^{n_3} 2E_3 (2\pi)^3 \delta^3(\mathbf{p}_3 - \mathbf{p}_3^l) \sum_{m=1}^{n_4} 2E_4 (2\pi)^3 \\ &\quad \times \delta^3(\mathbf{p}_4 - \mathbf{p}_4^m) |\langle p_1' \dots p_n'; p_3^1 \dots p_3^{n_3}; p_4^1 \dots p_4^{n_4} | A | p_1 p_2 \rangle|^2 \end{aligned} \tag{10.3.12}$$

Then like (10.3.7)

$$\begin{aligned} \int f_2(\mathbf{p}_3, \mathbf{p}_4, s) \frac{d^3\mathbf{p}_3}{16\pi^3 E_3} \frac{d^3\mathbf{p}_4}{16\pi^3 E_4} &= \sigma(1 + 2 \rightarrow 3 + 4 + X') \\ &\quad + 2\sigma(1 + 2 \rightarrow 3 + 3 + 4 + X') + 2\sigma(1 + 2 \rightarrow 3 + 4 + 4 + X') \\ &\quad + 4\sigma(1 + 2 \rightarrow 3 + 3 + 4 + 4 + X') + \dots \\ &\equiv \langle n_3 n_4 \rangle \sigma_{12}^{\text{tot}}(s) \end{aligned} \tag{10.3.13}$$

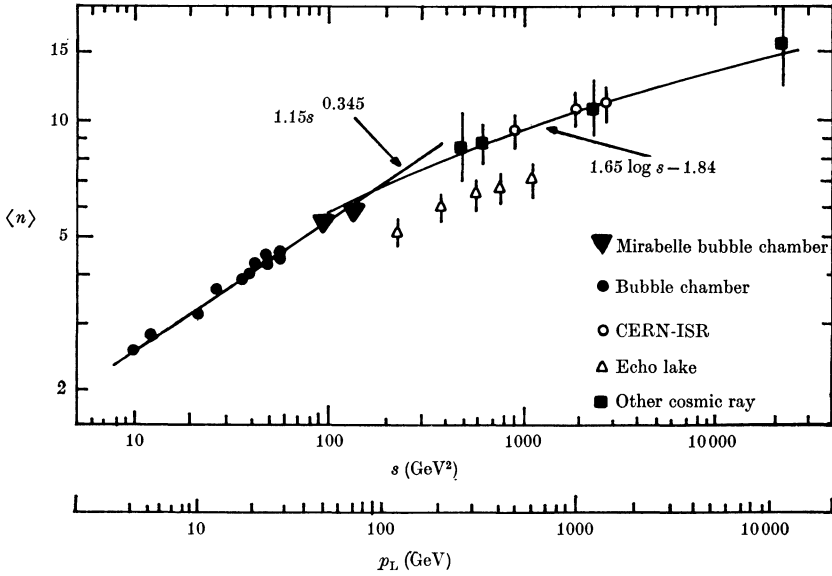


FIG. 10.5 The average charged multiplicity $\langle n \rangle$ in pp scattering versus s , showing the logarithmic increase, from Morrison (1972).

where X' includes no particle of type 3 or 4, and where $\langle n_3 n_4 \rangle$ is the average of the product of the multiplicities of 3 and 4. This assumes that 3 and 4 are distinct types of particles (for example 3 might be pions and 4 protons, or 3 might be negatively charged particles and 4 positively charged ones). If 3 and 4 are the same type of particle then

$$\int f_2(\mathbf{p}_3, \mathbf{p}_4, s) \frac{d^3 \mathbf{p}_3}{16\pi^3 E_3} \frac{d^3 \mathbf{p}_4}{16\pi^3 E_4} = 2\sigma(1 + 2 \rightarrow 3 + 3 + X') + 6\sigma(1 + 2 \rightarrow 3 + 3 + 3 + X') + \dots \equiv \langle n_3(n_3 - 1) \rangle \sigma_{12}^{tot}(s) \quad (10.3.14)$$

since in a given event producing n_3 particles of type 3 there are n_3 different ways of choosing the first particle to be detected, and $n_3 - 1$ ways of choosing the second particle.

Similar to (10.3.10) we can define

$$\rho_2(\mathbf{p}_3, \mathbf{p}_4, s) \equiv \frac{f_2(\mathbf{p}_3, \mathbf{p}_4, s)}{\sigma_{12}^{tot}(s)} \quad (10.3.15)$$

and combining (10.3.13) and (10.3.14) we find

$$F_2(s) \equiv \int \rho_2 \frac{d^3 \mathbf{p}_3}{16\pi^3 E_3} \frac{d^3 \mathbf{p}_4}{16\pi^3 E_4} = \langle n_3 n_4 - \delta_{34} n_3 \rangle \quad (10.3.16)$$

These results are readily generalized to give the inclusive distributions for producing any number of types of particles, m , in the process $1 + 2 \rightarrow 3 + 4 + \dots (m + 2) + X$, for which

$$F_m(s) \equiv \int \rho_m \prod_{i=3}^{m+2} \frac{d^3\mathbf{p}_i}{16\pi^3 E_i} = \langle n_3(n_3 - 1) \dots (n_3 - m + 1) \rangle \tag{10.3.17}$$

if 3, 4, ..., $(m + 2)$ are all the same type of particle, where

$$\rho_m(\mathbf{p}_3 \dots \mathbf{p}_{m+2}, s) \equiv \frac{1}{\sigma_{12}^{\text{tot}}} (16\pi^3)^m E_3 \dots E_{m+2} \frac{d^{3m}\sigma}{d^3\mathbf{p}_3 \dots d^3\mathbf{p}_{m+2}} \tag{10.3.18}$$

Since we do not observe most of the final-state particles, X , it might be thought that these inclusive measurements must always provide less information about the scattering process than exclusive measurements in which all the particles are observed, but this is not really so.

We can write the exclusive cross-section for $a + b \rightarrow 1 + \dots + n$ (fig. 10.6) as

$$(16\pi^3)^n E_1 \dots E_n \frac{d^{3n}\sigma^{\text{ex}}}{d^3\mathbf{p}_1 \dots d^3\mathbf{p}_n}$$

but if we observe, say, only l of these, the inclusive cross-section for $a + b \rightarrow l + X$ is

$$(16\pi^3)^l E_1 \dots E_l \frac{d^{3l}\sigma^{\text{in}}}{d^3\mathbf{p}_1 \dots d^3\mathbf{p}_l} = \sum_{n=l}^{\infty} \frac{1}{(n-l)!} \int (16\pi^3)^l \times E_1 \dots E_l \frac{d^{3n}\sigma^{\text{ex}}}{d^3\mathbf{p}_1 \dots d^3\mathbf{p}_n} d^3\mathbf{p}_{l+1} \dots d^3\mathbf{p}_n \tag{10.3.19}$$

if we treat all the n particles as identical. So, as expected, the inclusive cross-sections can be obtained from the exclusive ones. But conversely a given n -particle exclusive cross-section can be obtained from all the $n + l$ inclusive ones, since

$$(16\pi^3)^n E_1 \dots E_n \frac{d^{3n}\sigma^{\text{ex}}}{d^3\mathbf{p}_1 \dots d^3\mathbf{p}_n} = \sum_{l=0}^{\infty} \frac{(-l)!}{l!} \int (16\pi^3)^n \times E_1 \dots E_n \frac{d^{3(n+l)}\sigma^{\text{in}}}{d^3\mathbf{p}_1 \dots d^3\mathbf{p}_{n+l}} d^3\mathbf{p}_{n+1} \dots d^3\mathbf{p}_{n+l} \tag{10.3.20}$$

The counting is explained for $n = 3$ in fig. 10.7: we take the three-body inclusive process, but subtract all those processes where at least four bodies are produced, remembering that because of the identity of the particles the five-body exclusive cross-section contributes $2!$ times to the three-body inclusive cross-section; and so on.

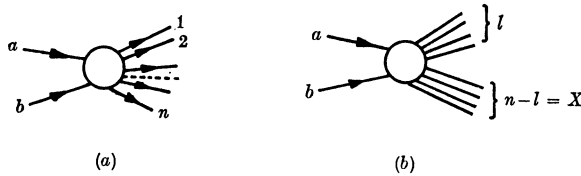


FIG. 10.6 (a) The n -body exclusive cross-section. (b) Contribution of the n -body final state to the l -particle inclusive cross-section.

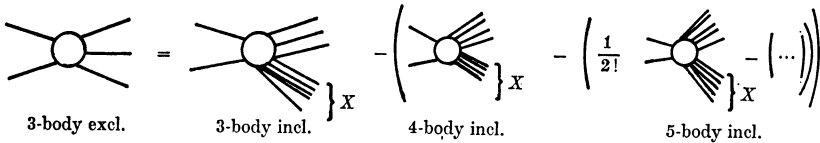


FIG. 10.7 The three-body exclusive cross-section in terms of three- and more-body inclusive cross-sections, as in (10.3.20).

Hence the complete set of inclusive cross-sections contains exactly the same information as the complete set of exclusive ones. Of course many-body inclusive cross-sections are too hard to measure and analyse, as are many-body exclusive cross-sections, and so in practice few-body inclusive cross-sections give complementary information to few-body exclusive ones.

The next step is to derive Mueller’s theorem which allows us to make Regge predictions for these inclusive distributions.

10.4 Mueller’s generalized optical theorem

In section 1.9, and graphically in fig. 1.6, we gave a derivation of the optical theorem relating the total cross-section $\sigma(12 \rightarrow X)$ to the imaginary part of the forward elastic amplitude $A^{el}(12 \rightarrow 12)$. Mueller (1970) has obtained a generalization of this result which provides the basis for Regge predictions of inclusive distributions. This is shown in fig. 10.8 and gives

$$f_1(\mathbf{p}_3, s) = \frac{1}{2q_s\sqrt{s}} \text{Disc}_X\{A(12\bar{3})\} \rightarrow \frac{1}{s} \text{Disc}_X\{A(12\bar{3})\} \quad (10.4.1)$$

where $A(12\bar{3})$ is the amplitude for the process $1 + 2 + \bar{3} \rightarrow 1' + 2' + \bar{3}'$.

In the first step we use the completeness relation for $\Sigma|A(12 \rightarrow 3X)|^2$. The second step uses the crossing property of section 1.6 to analytically continue the amplitude from an outgoing 3 to an incoming $\bar{3}$; and then the unitarity relation (1.9.3) is used to relate this to the discontinuity

$$\begin{aligned}
 f_1 &= \frac{1}{4q_s\sqrt{s}} \sum_X \left| \begin{array}{c} 1 \quad 3 \\ \circlearrowleft \quad \circlearrowright \\ 2 \quad X \end{array} \right| 2 = \frac{1}{4q_s\sqrt{s}} \sum_X \left(\begin{array}{c} 1 \quad 3 \quad 3' \quad 1' \\ \circlearrowleft \quad A \quad \text{---} \quad A^\dagger \quad \circlearrowright \\ 2 \quad X \quad 2' \end{array} \right) \\
 &= \frac{1}{4q_s\sqrt{s}} \sum_X \left(\begin{array}{c} \bar{3} \quad \bar{3}' \\ 1 \quad 1' \\ 2 \quad 2' \end{array} \right) = \frac{1}{2q_s\sqrt{s}} \text{Disc } X \left\{ \begin{array}{c} \bar{3} \\ 1 \\ 2 \end{array} \right\}
 \end{aligned}$$

(a) (b)

(c) (d)

FIG. 10.8 Derivation of Mueller's theorem. (a) is the definition of f_1 , where $4q_s\sqrt{s}$ is the flux factor (1.8.4). To get (b) we use the completeness relation, then (c) is obtained by crossing 3 and 3', and (d) is the unitarity relation for the $3 \rightarrow 3$ amplitude. (The factor 2 arises from the definition (10.4.2).)

of the forward elastic scattering amplitude for $12\bar{3} \rightarrow 12\bar{3}$ in the variable

$$M_X^2 = M^2 = (p_1 + p_2 - p_3)^2 = s_{123}$$

Here

$$\text{Disc}_X \{ A(12\bar{3}; s_{12\bar{3}}, s, t) \} \equiv \frac{1}{2i} (A(12\bar{3}; s_{12\bar{3}} + i\epsilon, s, t) - A(12\bar{3}; s_{12\bar{3}} - i\epsilon, s, t)) \tag{10.4.2}$$

i.e. the discontinuity is taken across the $s_{12\bar{3}}$ branch cut but keeping on the same side of cuts in s and t . Since the initial state has to be identical to the final state we must have $t_{11'} = t_{22'} = t_{33'} = 0$ (where $t_{11'} \equiv (p_1 - p_1')^2$, etc.) just as we needed $t = 0$ in (1.9.6).

The obvious problem associated with this derivation, which is not present with fig. 1.6, is that we have had to make an analytic continuation in p_3 to the unphysical scattering amplitude $A(12\bar{3})$, and we cannot be sure whether the discontinuity will be affected by so doing. The discontinuity in (10.4.2) is across M^2 keeping on the same side of the cuts in $s \equiv s_{12}$, whereas clearly in fig. 10.8(b) we are above the threshold cut in this variable in A but below it at A^\dagger . The independence of normal-threshold discontinuities mentioned in section 9.3 guarantees that the discontinuity in the one variable is unaffected by taking the discontinuity across the other, but anomalous thresholds etc. could spoil the result. However, the general consensus of informed opinion seems to be that this is unlikely (see Cahill and Stapp 1972, 1973, Polkinghorne 1972).

Even so this generalization is clearly more difficult to use than the ordinary optical theorem because in (1.9.6) the total cross-section for a given p_1 and p_2 is related to the elastic amplitude for the same physical values of p_1 and p_2 , but (10.4.1) relates the inclusive distribution for $1 + 2 \rightarrow 3 + X$ to the (in any case unmeasurable) process $1 + 2 + \bar{3} \rightarrow 1 + 2 + \bar{3}$ in an unphysical region of $p_{\bar{3}}$. However, even if we cannot measure $A(12\bar{3})$ we can certainly write down a Regge parameterization for it, just as we used the Regge parameters of $A^{\text{el}}(12)$ to predict the behaviour of $\sigma_{12}^{\text{tot}}(s)$ in (6.8.4). It is this which makes inclusive reactions such a valuable testing ground for Regge theory, as we shall see in the following sections.

So far we have neglected the spins of the particles. More strictly we should average over the possible helicities of 1 and 2, and sum over those of 3, so (10.3.2) gives

$$\begin{aligned}
 f_1(\mathbf{P}_3, s) &= \frac{1}{4q_s \sqrt{s} (2\sigma_1 + 1) (2\sigma_2 + 1)} \sum_X \sum_{\mu_1 \mu_2 \mu_3} |A_{\mu_1 \mu_2 \mu_3}(12 \rightarrow 3X)|^2 \\
 &= \frac{1}{2q_s \sqrt{s} (2\sigma_1 + 1) (2\sigma_2 + 1)} \\
 &\quad \times \sum_{\mu_1 \mu_2 \mu_3} \text{Disc}_X [\langle \mu_1 \mu_2 \mu_3 | A(12\bar{3} \rightarrow 12\bar{3}) | \mu_1 \mu_2 \mu_3 \rangle] \quad (10.4.3)
 \end{aligned}$$

through the optical theorem (10.4.1). So far, rather few polarization or density matrix measurements have been made, so we shall simply neglect spin below, which means strictly that at each Reggeon vertex we are averaging over the different possible helicities. But if for example 3 has spin = $\frac{1}{2}$, its polarization P_{3y} is given by (cf. (4.2.22))

$$\begin{aligned}
 P_{3y} f_1(\mathbf{P}_3, s) &= \frac{1}{4q_s \sqrt{s} (2\sigma_1 + 1) (2\sigma_2 + 1)} \\
 &\quad \times \sum_{\mu_1 \mu_2} \text{Im} \{ \text{Disc}_X [\langle \mu_1 \mu_2 - | A(12\bar{3} \rightarrow 12\bar{3}) | \mu_1 \mu_2 + \rangle] \} \quad (10.4.4)
 \end{aligned}$$

where $\pm \equiv \pm \frac{1}{2}$. Alternatively inclusive density matrices can be defined like (4.2.10) and clearly they will tell us about the helicity dependence of the Reggeons' couplings to the particles (see Phillips, Ringland and Worden 1972, Goldstein and Owens 1975).

10.5 Fragmentation and the single-Regge limit

In the region where x_3 or $\tilde{y}_3 \approx 1$, i.e. particle 3 is almost at rest in the Lorentz frame of particle 1, we can regard 3 as a fragment of 1, as in fig. 10.3(a). This is called the 'fragmentation region' of 1, and the

inclusive distribution in this region is sometimes written as $f_1(1 \xrightarrow{2} 3)$, i.e. $1 \rightarrow 3$ under the impact of 2. Indeed 3 may well be the same particle as 1, since then no quantum numbers need be exchanged. The frequent occurrence of the beam particle in the final state, with high p_L but small p_T , and hence close to the forward direction, is called the 'leading particle effect'.

So in this region we are concerned with high energies, $s = s_{12} \rightarrow \infty$, but $t = t_{13}$ fixed and small. And from (10.2.14) fixed x_3 implies $M^2 \rightarrow \infty$ with fixed M^2/s . Now M^2 is the total energy for the $ab\bar{c}$ elastic scattering process in fig. 10.8(d), and large M^2 , small t suggests a single Regge pole exchange picture as in fig. 10.9(a), so we write

$$f_1(1 \rightarrow 3; \mathbf{p}_3, s) = \sum_i \gamma_i \left(t, \frac{M^2}{s} \right) \left(\frac{M^2}{s_0} \right)^{\alpha_i(0)-1} \quad (10.5.1)$$

where we have summed over all the Reggeons which can be exchanged. The argument of α_i is 0 because always $t_{22'} = 0$ for this forward three-body process. It should not be confused with $t \equiv t_{13}$ which gives the (fixed) invariant mass of the quasi-particle ($1\bar{3}$). From the similarity of fig. 9.1(a) to fig. 9.1(b) it is evident from (9.2.30) and (9.2.31) that the value of M^2/s determines the angle between the planes containing $1\bar{3}$ and $2\bar{3}$. In (10.5.1) s_0 is the usual scale factor, which experience with $2 \rightarrow 2$ scattering suggests should be $\approx 1 \text{ GeV}^2$. We neglect the possibility of Regge cuts which would modify (10.5.1) by $\log(M^2)$ factors.

The validity of this formula depends on

$$s, M^2 \text{ and } u = (p_2 - p_3)^2 \gg m_3^2, t \text{ and } s_0.$$

So we need s large as usual, and $M^2/s = 1 - x$ finite; so M^2 must be large also, but not too large since $M^2 \rightarrow s$ implies $x \rightarrow 0$ (and from (10.2.12) u becomes small) so we would leave the fragmentation region. Obviously for $x_3, \tilde{y}_3 \approx -1$ we have the process $2 \xrightarrow{1} 3$, i.e. 3 is a fragment of 2, and the Regge picture is fig. 10.9(b), so we can account for both fragmentation regions. But clearly it is necessary for these two regions to be well separated, which, as we shall show below (section 10.10) needs $Y = y_{\max} - y_{\min} > 4$, or $s > 60 \text{ GeV}^2$, from (10.2.25).

In an elastic scattering process the dominant exchange should be the Pomeron, P, and if $\alpha_P(0) \approx 1$ we have

$$f_1(\mathbf{p}_3, s) \xrightarrow{s \rightarrow \infty} \gamma_P \left(t, \frac{M^2}{s} \right) \quad (10.5.2)$$

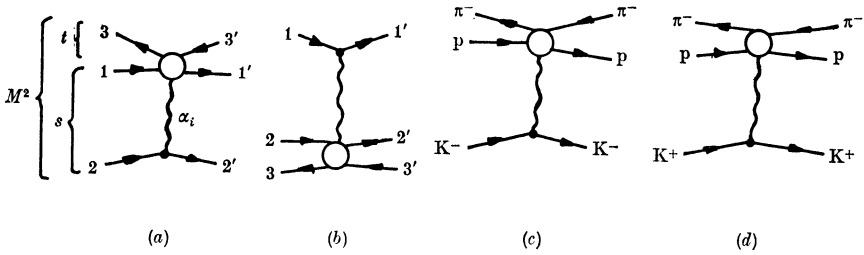


FIG. 10.9 (a) The Regge exchange diagram for $\text{Disc}_X\{A(12\bar{3} \rightarrow 12\bar{3})\}$ when 3 is in the fragmentation region of 1, i.e. $t_{13} = (p_1 - p_3)^2$ is small. (b) The corresponding diagram for the 2-fragmentation region. (c), (d) The Mueller-Regge diagrams for $p \rightarrow \pi^+$.

and so, like $\sigma_{12}^{\text{tot}}(s), f_1(\mathbf{p}_3, s)$ should be approximately independent of s for $s \rightarrow \infty, t, M^2/s$ fixed, i.e. f_1 should ‘scale’.

A cross-section is said to ‘scale’ if its numerical value is independent of the energy units which are used. Thus $\sigma_{12}^{\text{tot}}(s)$ has values which when expressed as a function of s are independent of the units in which s is measured only if σ_{12}^{tot} is independent of s , which is approximately true at high energies. Likewise in (10.5.2) $f_1 = f_1(t, M^2/s)$ only, so though it depends on s at fixed M^2 (and vice versa) any change of the units in which they are both measured will not affect the ratio M^2/s , so f_1 scales. This is not true generally of (10.5.1) of course.

This scaling result agrees with earlier predictions of Amati *et al.* (1962*a, b*), Yang and co-workers (Benecke *et al.* 1969) and Feynman (1969). Yang’s prediction was based on the hypothesis of limiting fragmentation, i.e. that the distribution of 3 in the rest frame of 1 should become independent of s for large s . This is because he viewed the scattering particles, 1 and 2, as two Lorentz-contracted disks passing through and exciting each other, followed by a break-up of each disk. Since $\sigma^{\text{el}}, \sigma^{\text{tot}} \rightarrow \text{constants}$, the forces between the disks are obviously not changing as $s \rightarrow \infty$, and so the break-up of each disk should reach a limiting distribution (in its own rest frame) with no multiple scattering. Feynman’s view, like that of Amati and co-workers, was based on the observation that in multi-peripheral and similar models (to be discussed in the next chapter) the distribution of 3 in x_3 and \mathbf{p}_{3T} becomes independent of s as $s \rightarrow \infty$. This agrees with Yang’s hypothesis and with the single-Regge limit (10.5.2) for $x_3^2 \gg 4\mu_3^2/s$, but extends the result down to $x = 0$ too, which we shall not deal with until the next section.

This scaling hypothesis works well in many processes. For example

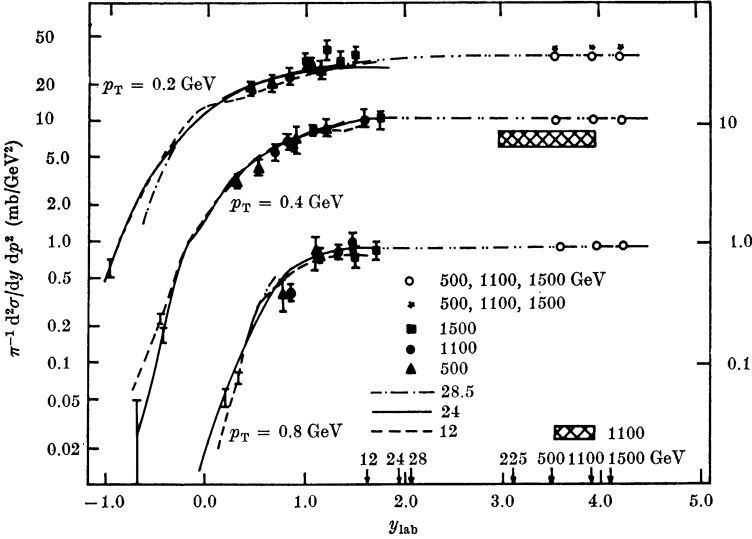


FIG. 10.10 Data for $pp \rightarrow \pi^+X$ in the fragmentation region, from Morrison (1972).

in $pp \rightarrow \pi^+X$, shown in fig. 10.10, we see that f_1 is independent of s in the fragmentation region for $s = 50 \rightarrow 3000 \text{ GeV}^2$. Of course $\sigma_{pp}^{\text{tot}}(s)$ is not constant at high s , so that effectively $\alpha_P(0) > 1$, and it might be expected that ρ_1 (defined in (10.3.10)), rather than f_1 , would be the better distribution in which to observe scaling, but generally the data are not sufficiently accurate to distinguish these possibilities.

The great advantage of this Regge view of scaling is that it also predicts how fast the scaling behaviour will be reached (Brower *et al.* 1973*a*, Chan *et al.* 1972*b*) provided we neglect cuts. The next term in the series (10.5.1) will be the normal Reggeons $R = f, \omega, \rho, A_2$ all with $\alpha_R(0) \approx 0.5$, and approximately equal couplings because of exchange degeneracy, so if they all add (as in $p \xrightarrow{K^-} \pi^-$, fig. 10.9(c)) we get

$$f_1(p_3, s) = \gamma_P \left(t, \frac{M^2}{s} \right) + 4\gamma_R \left(t, \frac{M^2}{s} \right) \left(\frac{M^2}{s_0} \right)^{-\frac{1}{2}} \quad (10.5.3)$$

If now we replace 2 by $\bar{2}$ (i.e. K^- is replaced by K^+ as in fig. 10.9(d)) the ω and ρ contributions change sign because they are odd under charge conjugation, giving

$$f_1(1 \rightarrow \bar{3}) - f_1(1 \rightarrow 3) = 4\gamma_R \left(t, \frac{M^2}{s} \right) \left(\frac{M^2}{s_0} \right)^{-\frac{1}{2}} \quad (10.5.4)$$

and comparing for example $p \rightarrow \pi^-$ and $p \rightarrow \pi^-$ gives $\gamma_R/\gamma_P \approx \frac{1}{3}$, so we need $s \approx 2000 \text{ GeV}^2$ for scaling to hold to within 10 per cent. However, we have found in two-body scattering that, because of duality, exchange degeneracy may result in a mutual cancellation of these secondary terms in exotic processes (see section 7.5), i.e. if $1+2$ have exotic quantum numbers, like K^+p , then scaling occurs precociously in $\sigma_{12}^{\text{tot}}(s)$, at very low values of s . We can expect this also to be true in inclusive reactions, i.e. that scaling will occur if $(12\bar{3})$ has exotic quantum numbers so that no resonances occur in M^2 . However, this is only really analogous to $2 \rightarrow 2$ scattering if $(1\bar{3})$ is not exotic as well, so that we can treat it as a quasi-particle. A more systematic investigation is therefore needed, which we postpone to section 10.6.

As long as poles rather than cuts dominate we can get extra constraints on the inclusive distributions from factorization. Thus we can express fig. 10.9(a) in the form

$$f_1(1 \xrightarrow{2} 3; \mathbf{p}_3, s) = \sum_i \gamma_{22}^i G_{1\bar{3}}^i \left(t, \frac{M^2}{s} \right) \left(\frac{M^2}{s_0} \right)^{\alpha_i(0)-1} \tag{10.5.5}$$

where $\gamma_{22}^i = \gamma_{22}^i(t_{22'} = 0)$ is the Reggeon coupling to $2\bar{2}$ and $G_{1\bar{3}}^i$ represents the upper vertex. For $s \rightarrow \infty$ this becomes, with $\alpha_P(0) = 1$,

$$f_1(1 \xrightarrow{2} 3) \rightarrow \gamma_{22}^P G_{1\bar{3}}^P \left(t, \frac{M^2}{s} \right) \tag{10.5.6}$$

but we also have from (6.8.4)

$$\sigma_{12}^{\text{tot}}(s) = \sum_i \gamma_{11}^i \gamma_{22}^i s^{\alpha_i(0)-1} \rightarrow \gamma_{11}^P \gamma_{22}^P \tag{10.5.7}$$

so from (10.3.10)
$$\rho_1(1 \xrightarrow{2} 3) \rightarrow \frac{G_{13}^P(t, M^2/s)}{\gamma_{11}^P} \tag{10.5.8}$$

which is independent of particle 2, and so $\rho_1(1 \xrightarrow{a} 3)$ should be independent of a for $s \rightarrow \infty$. This can be tested at finite energies only for exotic $(12\bar{3})$ processes which scale early, such as $p \rightarrow \pi^-$, $p \rightarrow \pi^-$, $p \rightarrow \pi^-$, and it is found (see fig. 10.11) that ρ_1 is the same for all three.

The secondary contributions are also related by the exchange degeneracy of the couplings (Miettinen 1972, Chan *et al.* 1972a). Thus

$$f_1(p \rightarrow \pi^-) = \gamma_{\pi^+\pi^+}^P G_{p\pi^+}^P + \gamma_{\pi^+\pi^+}^f G_{p\pi^+}^f \left(\frac{M^2}{s_0} \right)^{-\frac{1}{2}} - \gamma_{\pi^+\pi^+}^p G_{p\pi^+}^p \left(\frac{M^2}{s_0} \right)^{-\frac{1}{2}} \tag{10.5.9}$$

where the negative sign of the last term is due to the fact that $\pi^+\pi^+$ is

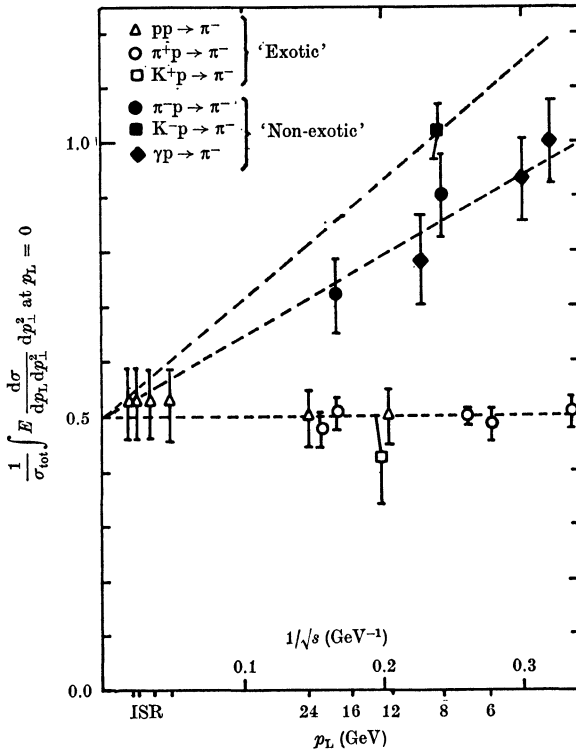


FIG. 10.11 The energy dependence of ρ_1 (equation (10.5.8)) integrated over p_{3T}^2 for a variety of processes, showing that it is independent of particle 2, at least for exotic channels, from Miettinen (1973).

exotic (and π^+p is not) so that these secondary f and ρ terms should cancel. But from $\pi^+\pi^+ \rightarrow \pi^+\pi^+$ we know that $\gamma_{\pi^+\pi^+}^f = \gamma_{\pi^+\pi^+}^\rho$ (see (7.5.2)) so we must also have

$$G_{p\pi^+}^\rho = G_{p\pi^+}^f \tag{10.5.10}$$

Similarly on considering $p \xrightarrow{K^+} \pi^-$ and $p \xrightarrow{K^-} \pi^-$ we deduce that

$$G_{p\pi^+}^f = G_{p\pi^+}^\omega = G_{p\pi^+}^{A_s}$$

and that all γ_{KK}^R are equal and hence

$$f_1(p \rightarrow \pi^-)^{K^-} - f_1(p \rightarrow \pi^-)^{K^+} = 4\gamma_{KK}^R G_{p\pi^+}^R \left(\frac{M^2}{s_0}\right)^{-\frac{1}{2}} \tag{10.5.11}$$

And for any similar fragmentation we can write

$$f_1(p \rightarrow \pi^-)^a = \gamma_{aa}^P G_{p\pi^+}^P + \sum_R \gamma_{aa}^R G_{p\pi^+}^R \left(\frac{M^2}{s_0}\right)^{-\frac{1}{2}} \tag{10.5.12}$$

so, since the behaviour of $\sigma_{\text{ap}}^{\text{tot}}$ allows us to deduce γ_{aa}^{R} , we can predict all $f_1(\text{p} \xrightarrow{a} \pi^-)$. This is found to work well for $a = \gamma, \text{K}^-$ or π^- for example.

Factorization is much more useful in inclusive reactions than in two-body processes because the target is effectively ($\bar{1}\bar{3}$). Thus even if the actual target (particle 1) is restricted to p or (n) we can still change both vertices in fig. 10.9(a) by changing the beam particle (2) and particle 3.

It is rather remarkable that these factorization tests should work so well, though of course the data are not very accurate in general. It may partly be explained by the fact that we are restricted to $t_{22'} = 0$ where the poles are more important, or it may be the result of pole-enhancement of the cuts (see section 8.7g).

10.6 The central region and the double-Regge limit

We consider next the region $x \approx 0$ where $p_{3\text{L}}$ is small. As $s \rightarrow \infty$ we have, from (10.2.10) and (10.2.11),

$$t \rightarrow -(\sqrt{s})(E_3 - p_{3\text{L}}), \quad u \rightarrow -(\sqrt{s})(E_3 + p_{3\text{L}}) \tag{10.6.1}$$

so that $|t|, |u| \rightarrow \infty$ as $s \rightarrow \infty$, but

$$\frac{ut}{s} \rightarrow (E_3 - p_{3\text{L}})(E_3 + p_{3\text{L}}) = \mu_3^2 \tag{10.6.2}$$

is fixed. So like η_{12} in (9.2.31), μ_3^2 represents the angle between the plane containing 1 and 3 and the plane containing 2 and 3. Since μ_3^2 is generally small, $\leq 1 \text{ GeV}^2$, it requires a very large s to get large $|t|$ and $|u|$, particularly if m_3 is small.

The double-Regge exchange model for this region is shown in fig. 10.21 and gives

$$f_1(\mathbf{p}_3, s) = \sum_{i,j} \frac{1}{s} \gamma_{ij}(\mathbf{p}_{3\text{T}}) \left| \frac{t}{s_0} \right|^{\alpha_i(0)} \left| \frac{u}{s_0} \right|^{\alpha_j(0)} \left(\frac{s_0}{\mu_3^2} \right) \tag{10.6.3}$$

where γ_{ij} represents the product of the three vertices, and the extra factor (s_0/μ_3^2) is arbitrary but convenient, because using (10.6.2) we then get for $s \rightarrow \infty$

$$f_1(\mathbf{p}_3, s) \rightarrow \sum_{i,j} \gamma_{ij}(\mu_3^2) \left| \frac{t}{s_0} \right|^{\alpha_i(0)-1} \left| \frac{u}{s_0} \right|^{\alpha_j(0)-1} \tag{10.6.4}$$

If P dominates asymptotically this gives the Feynman scaling result (fig. 10.13(a))

$$f_1(\mathbf{p}_3, s) \rightarrow \gamma_{\text{PP}}(\mu_3^2) \tag{10.6.5}$$

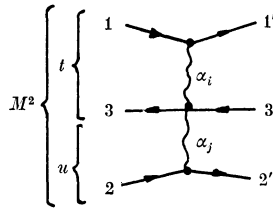


FIG. 10.12 Mueller-Regge diagram for the central region (equation (10.6.3)).

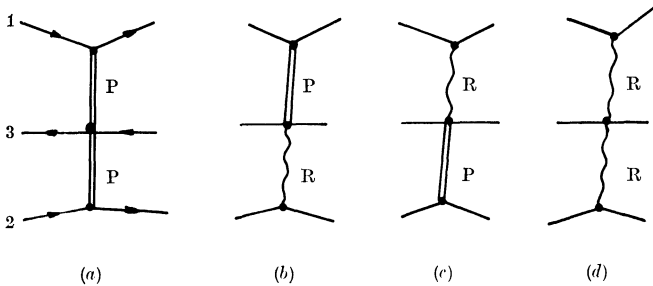


FIG. 10.13 Central region Mueller-Regge diagrams; (a) gives scaling asymptotically while the others give corrections to the scaling behaviour from R exchange.

independent of s , t and u (see fig. 10.14). Using factorization this can be rewritten as

$$f_1(\mathbf{p}_3, s) \rightarrow \gamma_{11}^P \gamma_{33}^{PP}(\mu_3^2) \gamma_{22}^P \quad (10.6.6)$$

or, using (10.3.10) and (10.5.7),

$$\rho_1(\mathbf{p}_3, s) \rightarrow \gamma_{33}^{PP}(\mu_3^2) \quad (10.6.7)$$

which is independent of particles 1 and 2. Also, since from (10.2.28) $y_3 \rightarrow \frac{1}{2} \log(u/t)$, this result means that $f_1(\mathbf{p}_{3T}, y_3, s)$ is independent of y_3 and s for small y_3 , i.e. $d\sigma/dy_3$ at fixed \mathbf{p}_{3T} will have a central plateau, as shown in fig. 10.4 (b). But for this to emerge from between the two fragmentation regions (each of width $\Delta y \approx 2$ - see section 10.10) we need $Y_3 \equiv y_{3\max} - y_{3\min} > 4$, so with $\mu_3^2 \approx 1 \text{ GeV}^2$ this means $s > 60 \text{ GeV}^2$.

The secondary Reggeons $R(= f, \omega, \rho, A_2)$ with $\alpha_R(0) \approx 0.5$ give corrections to scaling

$$\begin{aligned} f_1(\mathbf{p}_3, s) &= \gamma_{PP}(\mu_3^2) + \gamma_{PR}(\mu_3^2) \left| \frac{t}{s_0} \right|^{-\frac{1}{2}} \\ &\quad + \gamma_{RP}(\mu_3^2) \left| \frac{u}{s_0} \right|^{-\frac{1}{2}} + \gamma_{RR}(\mu_3^2) \left| \frac{t}{s_0} \right|^{-\frac{1}{2}} \left| \frac{u}{s_0} \right|^{-\frac{1}{2}} \\ &\sim \gamma_{PP}(\mu_3^2) + \gamma_{PR}(\mu_3^2) \left(\frac{s}{s_0} \right)^{-\frac{1}{4}} + O(s^{-\frac{1}{2}}) \end{aligned} \quad (10.6.8)$$

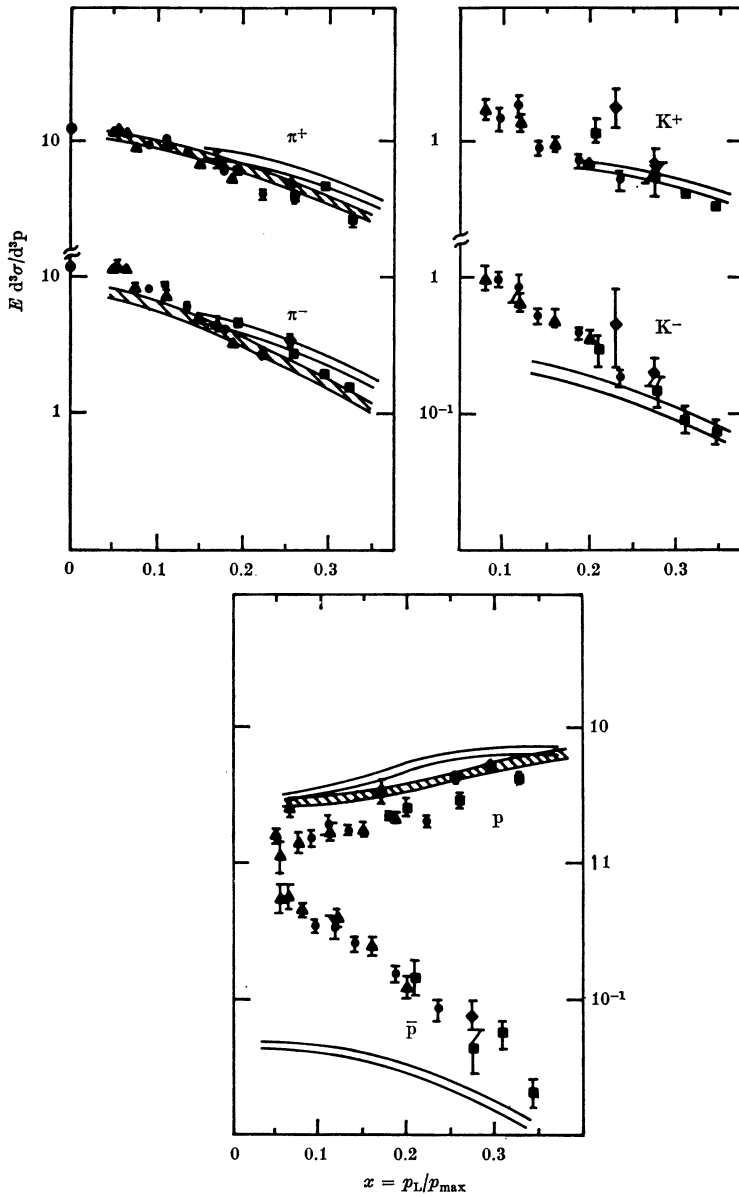


FIG. 10.14 Data for $pp \rightarrow \pi^+X$, $K^\pm X$, pX and $\bar{p}X$ in the central region showing the approximate scaling behaviour for π^\pm for high energies, from Jacob (1972).

since from (10.6.1) $t, u \sim \sqrt{s}$. According to Ferbel (1972) this $\sim s^{-\frac{1}{2}}$ approach to scaling works well at $x = 0$, but clearly this is very slow compared with the $\rightarrow s^{-\frac{1}{2}}$ approach in the fragmentation region. In $pp \rightarrow \pi^\pm X$ the cross-section rises with s up to $s \approx 1000 \text{ GeV}^2$, above which there is a fairly stable central plateau (fig. 10.14) but the cross-section is still rising slowly. However for $pp \rightarrow K^+, K^-, p$ or \bar{p} the plateau is still not well developed even at CERN-ISR, so it appears that only the very light pion is able to exhibit scaling even at the highest energies produced to date.

It seems natural that the cross-sections should all be rising with energy at low energies since it obviously becomes easier to produce heavy particles as the energy increases. But we have noted that $\langle n \rangle \sim \log s$ (section 10.3), which from (10.3.9) suggests that f_1 should be independent of y_3 , since $\sigma_{12}^{tot} \rightarrow \text{constant}$ and the range of y_3 to be integrated over, (10.2.25), increases like $\log s$. But there are positive non-scaling terms in the fragmentation region, so there must be negative non-scaling terms to cancel them in the central region, otherwise we would not get $\langle n \rangle \sim \log s$. Unfortunately, this effect is hard to reproduce in the Regge approach because the leading non-scaling terms, figs. 10.13 (b), (c) and (d), are expected to be positive from duality arguments. This is because they arise from the square of production amplitudes (fig. 10.15 (a)) which should be positive if resonances occur in X , and zero otherwise, just like the secondary contributions to $\sigma_{12}^{tot}(s)$. So the approach to scaling in the central region (10.6.8) should be from above too, according to Regge theory.

This difficulty led Chan *et al.* (1972a) to propose a new vacuum trajectory Q ($\alpha_Q(0) \approx 0.5$) with a negative coupling, so that fig. 10.5 (b) gives a negative contribution $f_1 \sim -\gamma_{QP} |t/s_0|^{-\frac{1}{2}}$. This is supposed to represent threshold effects, i.e. the difficulty of producing heavy particles in the central region. But really the fact that most cross-sections are still rising must be regarded as evidence that the Mueller-Regge approach is not yet fully applicable in the central region.

The normal secondary trajectories, R , can be observed by taking cross-section differences, such as fig. 10.16 for $\pi^+p \rightarrow \pi^+X$. Since the ρ coupling changes sign under $\pi^+ \leftrightarrow \pi^-$ we have

$$f(\pi^+p \rightarrow \pi^+X) - f(\pi^+p \rightarrow \pi^-X) = 2\gamma_{RP} \left| \frac{s}{s_0} \right|^{-\frac{1}{2}} \equiv \Delta(\pi^+p \rightarrow \pi^+X) \quad (10.6.9)$$

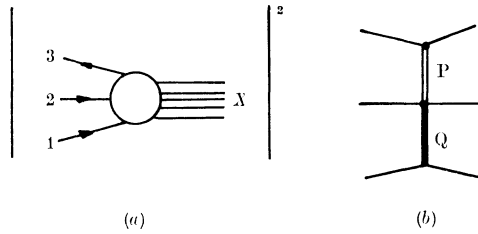


FIG. 10.15 (a) The (unphysical) production amplitude whose square contributes to the inclusive distribution. (b) The Q exchange which has been invented to parameterize threshold effects.

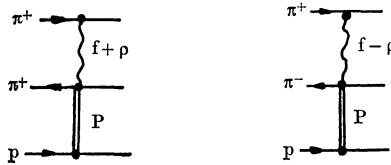


FIG. 10.16 Signs of the R contributions to fig. 10.13 (c) for $\pi^+p \rightarrow \pi^\pm X$.

Then using factorization to write (in a notation obvious from fig. 10.16)

$$\gamma_{RP}(\pi^+p \rightarrow \pi^-X) = \gamma_{\pi^+\pi^+}^R \gamma_{\pi^-\pi^-}^{RP} \gamma_{pp}^P$$

etc., we must have $\gamma_{\pi^-\pi^-}^{RP} = -\gamma_{\pi^+\pi^+}^{RP}$ from duality. A generalization allows one to deduce, from SU(3) and exchange degeneracy for the couplings, relations such as

$$\frac{\Delta(\pi^\pm p \rightarrow \pi^+ X)}{\Delta(pp \rightarrow \pi^+ X)} = \frac{1}{2} \left(\frac{\gamma_{\pi^+\pi^+}^P}{\gamma_{pp}^P} \pm \frac{\gamma_{\pi^-\pi^-}^P}{\gamma_{pp}^P} \right), \quad \frac{\Delta(K^\pm p \rightarrow \pi^+ X)}{\Delta(pp \rightarrow \pi^+ X)} = \frac{1}{2} \left(\frac{\gamma_{K^+K^+}^P}{\gamma_{pp}^P} \pm \frac{\gamma_{K^0K^0}^P}{\gamma_{pp}^P} \right) \tag{10.6.10}$$

where we have defined $\Delta(12 \rightarrow 3X) \equiv f(12 \rightarrow 3X) - f(12 \rightarrow \bar{3}X)$. These work well even at quite low energies (Inami 1974) which suggests that extracting the kinematic Q effect in $I = 0$ makes sense, even if one cannot take it seriously as a Regge pole. So it must be the $I = 0$ exchange part which has not yet developed its asymptotic behaviour.

Since in the central region f_1 depends on $\gamma_{ij}(\mu_3^2)$ in (10.6.4) (where μ_3 is defined in (10.2.2)) and since experimentally it is found that $f_1 \sim e^{-4p_T^2}$ for small p_T (see fig. 10.17), we can expect

$$\gamma_{ij} \sim e^{-4\mu_3^2} \tag{10.6.11}$$

So the coupling should be strongly dependent on the mass of the particle which is produced. Substituting m_3^2 for μ_3^2 gives the ratio of $\pi:K:p(\bar{p})$ production as 80:15:5 per cent which is at least qualitatively correct.

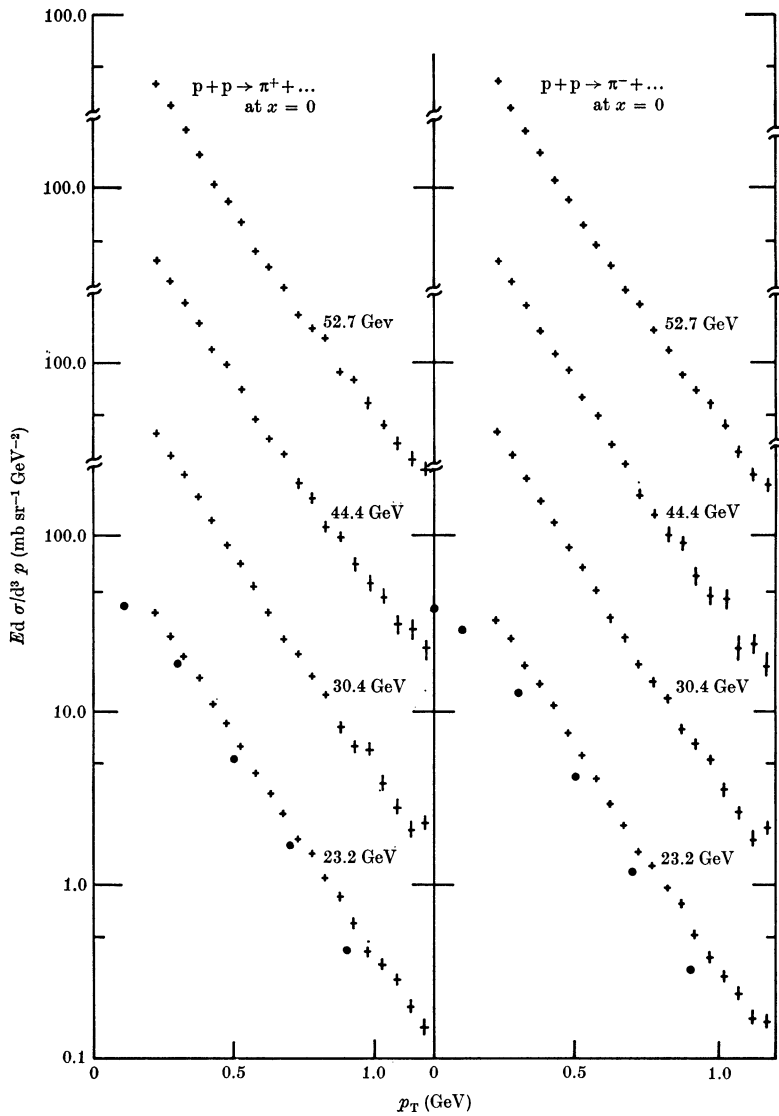
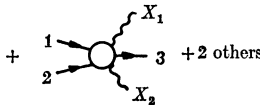
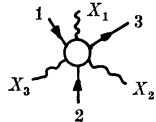
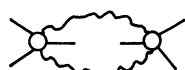
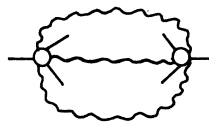


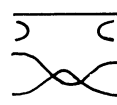
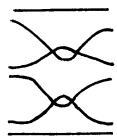
FIG. 10.17 The p_T dependence of f_1 for $pp \rightarrow \pi^\pm X$, showing the sharp cut-off in p_T , from Jacob (1972).

(a) $A(1\ 2\ \bar{3} \rightarrow X) =$  $+ 2\ \text{others}$

$+$  $+ 2\ \text{others}$ $+$ 

(b) $f_1 \propto \left| A(1\ 2\ \bar{3} \rightarrow X) \right|^2 =$  $+ 2\ \text{others}$

$+$  $+ 2\ \text{others}$ $+$ 

$=$  $+$  $+$ 

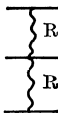
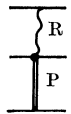
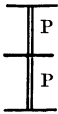
$=$  $+$  $+$ 

FIG. 10.21 (a) The seven terms for $A(12\bar{3} \rightarrow X)$. In each case the ‘others’ are just cyclically inequivalent permutations of the particles. (b) The seven corresponding contributions to the inclusive distribution f_1 , again excluding cross terms. They are redrawn below as duality diagrams, and as Reggeon and Pomeron exchanges.

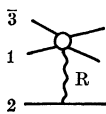
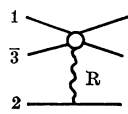
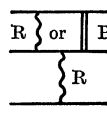
 $+$  $=$ 

FIG. 10.22 Single Regge diagrams for $1 \rightarrow \bar{3}$, and the corresponding duality diagrams.

rules for drawing duality diagrams (section (7.5)). A quark loop cannot begin and end on the same particle. So in accord with the Harari-Freund conjecture there are just two terms in σ_{12}^{tot} (see (7.3.1)).

Correspondingly, according to Veneziano (1972) there are seven terms in $12\bar{3} \rightarrow X$, shown in fig. 10.21 (a), and so if we neglect all cross terms the contributions to f_1 through the generalized optical theorem (10.4.1) are as shown in fig. 10.21 (b).

Strictly we get precocious scaling if the last term only is present, which requires that 12 , $2\bar{3}$ and $1\bar{3}$ are all exotic. But in the fragmentation region of particle 1 only figs. 10.22 matter. These cannot occur if 12 and $3\bar{2}$ are exotic giving early scaling in this region. A more complete discussion has been given by Einhorn *et al.* (1972b) and Tye and Veneziano (1973). Table 10.1 shows a comparison of exoticity and scaling in current data, from which it will be seen that if $\bar{3}$ is a π^\pm the criterion $12\bar{3}$ exotic seems to work, even if $1\bar{3}$ is exotic and so cannot form a quasi-particle, but on the other hand $pp \rightarrow \bar{p}X$ seems to violate all the rules, presumably because for such a heavy particle very high energies will be needed before there is sufficiently copious $\bar{p}p$ production for scaling to develop. It is the lightness of the pion which makes precocious scaling possible.

The fact that duality exchange-degeneracy relations between the Reggeon couplings seem to hold at quite low s in both the fragmentation and central regions suggests that it is the incomplete development of the P term which causes the difficulty.

10.8 Triple-Regge behaviour

In the fragmentation region $1 \rightarrow 3$, with a fixed M^2 and $s \rightarrow \infty$ we would expect Regge behaviour as shown in fig. 10.23 (a)

$$A(12 \rightarrow 3X) \xrightarrow{s \rightarrow \infty} \sum_i \gamma_{13}^i(t) \gamma_{2M}^i(t) \xi_i(t) P_{\alpha_i(t)}(\cos \theta_t) \tag{10.8.1}$$

where
$$\xi_i(t) = \frac{e^{-i\pi\alpha_i(t)} + \mathcal{G}_i}{\sin \pi\alpha_i(t)} \tag{10.8.2}$$

is the signature factor and $\gamma_{2M}^i(t)$ is the lower vertex of fig. 23 (a). If we insert (10.8.1) into the optical theorem (10.4.1), as in fig. 10.23 (b), we get

$$\begin{aligned} f_1(P_3, s) &= \frac{1}{2q_s \sqrt{s}} \text{Disc}_{M^2} \{A(12\bar{3} \rightarrow 12\bar{3})\} \rightarrow \frac{1}{s} \sum_{i,j} \gamma_{13}^i(t) \gamma_{13}^{j*}(t) \\ &\times \xi_i(t) \xi_j^*(t) (\cos \theta_t)^{\alpha_i(t) + \alpha_j(t)} \\ &\times \text{Disc}_{M^2} \{A(i2 \rightarrow j2; t, M^2, t_{22'} = 0)\} \end{aligned} \tag{10.8.3}$$

Table 10.1 *Scaling behaviour and exoticity*

| 1 | 3 | Exotic? | | | | Scale? | | |
|---------|-----------|--------------|-----|-------------|-------------|------------------------|---------|------------------------|
| | | 12 $\bar{3}$ | 12 | 2 $\bar{3}$ | 1 $\bar{3}$ | p fragmentation region | Central | 1 fragmentation region |
| π^+ | π^+ | No | No | No | No | ↓ | ↓ | ↓ |
| | π^- | Yes | No | No | Yes | — | ↑↑ | ↓↓ |
| | K^0 | Yes | No | No | No | — | ↑↑ | ↓↓ |
| π^- | p | No | No | No | No | ↓ | ↓ | ↓ |
| | π^+ | Yes | No | No | Yes | ↓ | ↑ | ↓ |
| | π^- | No | No | No | No | ↓ | — | ↓ |
| K^+ | K^0 | No | No | No | No | ↑ | ↑↑ | ↑ |
| | π^+ | No | Yes | No | No | — | ↑↑ | |
| | π^- | Yes | Yes | No | Yes | — | ↑↑ | |
| K^- | K^0 | Yes | Yes | No | Yes | ↓ | — | ↓ |
| | π^+ | No | No | No | Yes | ↓ | ↑↑ | ↓↓ |
| | π^- | No | No | No | No | — | ↑↑ | ↑↑ |
| p | K^0 | No | No | No | No | ↓ | ↑↑ | ↓↓ |
| | π^+ | Yes | Yes | No | No | ↓ | ↑↑ | ↓↓ |
| | π^- | Yes | Yes | No | No | ↓ | ↑↑ | ↓↓ |
| | K^0 | Yes | Yes | No | No | ↑ | ↑↑ | ↑↑ |
| | \bar{p} | No | Yes | No | No | ↓ | ↓ | ↓ |
| | \bar{p} | Yes | Yes | Yes | Yes | ↓ | ↑ | |

For processes of the form $1 + p \rightarrow 3 + X$ we show the tendency of the inclusive distribution in the fragmentation region of the target p, the central region, and the fragmentation region of the beam (particle 1); ↑ means that the cross-section is increasing with energy, ↓ that it is decreasing, and — that an approximately constant scaling behaviour is found. A blank means that suitable data is not available. (Based on Zalewsky 1974.)

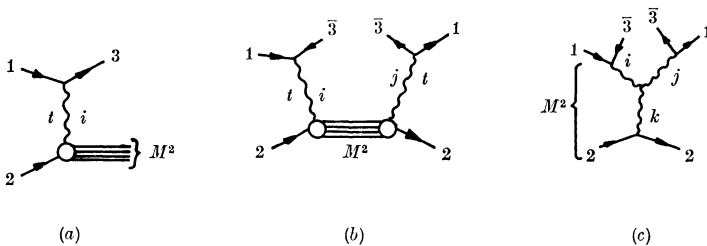


FIG. 10.23 (a) Single Reggeon i exchanged in $1 + 2 \rightarrow 3 + X$ when 3 is in the fragmentation region of 1, for large s . (b) The result of inserting (a) into the optical theorem, fig. 10.8. (c) The triple-Regge approximation to (b) appropriate at large M^2 . In (10.8.1) *et seq.* the Reggeon-particle couplings are denoted by γ_{13}^i etc. and the triple-Reggeon coupling in (c) is denoted by $\gamma^{ij,k}$.

where $A(i2 \rightarrow j2)$ is the Reggeon-particle scattering amplitude in the bottom half of the figure. Now if $s \gg M^2 \gg t \gg m_{1,2,3}^2$, from (1.7.19)

$$\cos \theta_t \rightarrow \frac{s - M^2/2}{q_{t13} q_{t2M}} \xrightarrow{s \gg M^2} \frac{s}{2q_{t13} q_{t2M}} \xrightarrow{M^2 \gg t} \frac{s}{M^2} \tag{10.8.4}$$

And for $M^2 \rightarrow \infty$ we can put (see fig. 10.23 (c))

$$\text{Disc}_{M^2}\{A(i2 \rightarrow j2)\} = \sum_k \gamma_{22}^k(0) \gamma^{ij,k}(t, 0) \left(\frac{M^2}{s_0}\right)^{\alpha_k(0)} \tag{10.8.5}$$

giving (from (10.3.4))

$$\begin{aligned} f_1(\mathbf{P}_3, s) &= 16\pi^2 s \frac{d^2\sigma}{dt dM^2} = \frac{1}{s} \sum_{i,j,k} \gamma_{13}^i(t) \gamma_{13}^{j*}(t) \\ &\quad \times \xi_i(t) \xi_j^*(t) \left(\frac{s}{M^2}\right)^{\alpha_i(t)+\alpha_j(t)} \gamma_{22}^k(0) \gamma^{ij,k}(t, 0) \left(\frac{M^2}{s_0}\right)^{\alpha_k(0)} \\ &\equiv \frac{1}{s} \sum_{i,j,k} G_{13, \frac{1}{2}}^{ij,k}(t) \left(\frac{s}{s_0}\right)^{\alpha_i(t)+\alpha_j(t)} \left(\frac{M^2}{s_0}\right)^{\alpha_k(0)-\alpha_i(t)-\alpha_j(t)} \end{aligned} \tag{10.8.6}$$

Note that the Reggeons i, j have mass $t \equiv (p_1 - p_3)^2$, but k has mass $t_{22} = 0$ since the optical theorem is for forward scattering. All the couplings and signature factors have been incorporated into $G_{13, \frac{1}{2}}^{ij,k}(t)$.

This expression is valid in the so-called ‘triple-Regge’ limit when M^2 and $s/M^2 \rightarrow \infty$. However, this is really a misnomer because, as we noted in section 10.5, s/M^2 gives the angle between the planes containing $\bar{13}$ and $\bar{23}$, and letting this angle tend to infinity is really a helicity limit in the language of section 9.3. However, the leading helicity pole occurs at $\lambda = \alpha$ (see (9.3.18)), so the fact that we are taking a mixed Regge-helicity pole limit in (10.8.6) does not make any difference to the formula to leading order in M^2 (see de Tar and Weis 1971).

From (10.2.14) we see that $s/M^2 \rightarrow \infty$ implies that $x_3 \rightarrow 1, y_3 \rightarrow y_{3 \max}$, so this triple-Regge region is only a small part of the x_3 or y_3 plot near the kinematical limit. Clearly (10.8.6) can only be applied for large s since if we suppose that we need $M^2/s_0 > 10$, and $s/M^2 > 10$ for the Regge expansion to be valid, with $s_0 = 1 \text{ GeV}^2$ this means $s > 100 \text{ GeV}^2$.

Using (10.2.14), (10.8.6) can be rewritten

$$f_1(\mathbf{P}_3, s) = \frac{1}{s} \sum_{i,j,k} G_{13, \frac{1}{2}}^{ij,k}(t) (1-x)^{\alpha_k(0)-\alpha_i(t)-\alpha_j(t)} \left(\frac{s}{s_0}\right)^{\alpha_k(0)} \tag{10.8.7}$$

and if M^2 is sufficiently large that only P is needed in the sum over k , and if the leading i and j trajectory with the quantum numbers of $\bar{13}$ is

denoted by i , then

$$\begin{aligned}
 f_1(\mathbf{p}_3, s) &\rightarrow \frac{1}{s} |\gamma_{13}^i(t)|^2 |\xi_i(t)|^2 \gamma_{22}^P(0) \gamma^{ii,P}(t, 0) \left(\frac{s}{M^2}\right)^{2\alpha_i(t)-1} \left(\frac{s}{s_0}\right) \\
 &\sim \left(\frac{s}{M^2}\right)^{2\alpha_i(t)-1} = (1-x)^{1-2\alpha_i(t)} \tag{10.8.8}
 \end{aligned}$$

so f_1 is a function of x , or M^2/s , only, which again corresponds to Feynman scaling. And by looking at the s variation at fixed M^2 , or the M^2 variation at fixed s , for different values of t , one can determine $\alpha_i(t)$ directly.

Rather comprehensive sets of fits of (10.8.6) to the high energy data have been made by Roy and Roberts (1974) and Field and Fox (1974). In $pp \rightarrow pX$, since $\overline{13} = \overline{pp}$ has the quantum numbers of the vacuum the leading term will be the triple-Pomeron term

$$f_1^{\text{PP,P}}(\mathbf{p}_3, s) = \frac{1}{s} G_{\text{PP,P}}^{\text{PP,P}}(t) \left(\frac{s}{s_0}\right)^{2\alpha_P(t)} \left(\frac{M^2}{s_0}\right)^{\alpha_P(0)-2\alpha_P(t)} \tag{10.8.9}$$

which with $\alpha_P(t) \approx 1 + \alpha'_P t$ gives

$$f_1^{\text{PP,P}} \approx \frac{1}{s_0} G_{\text{PP,P}}^{\text{PP,P}}(t) \left(\frac{s}{M^2}\right)^{1+2\alpha'_P t} \tag{10.8.10}$$

or, also from (10.8.6),

$$\frac{d^2\sigma}{dt dM^2} \approx \frac{G_{\text{PP,P}}^{\text{PP,P}}(t)}{16\pi^2 s_0} \frac{s^{2\alpha'_P t}}{(M^2)^{1+2\alpha'_P t}} \tag{10.8.11}$$

The secondary terms come from replacing i, j, k by R, where $\alpha_R(t) \approx 0.5 + \alpha'_R t$ so we can write

$$f_1 = f_1^{\text{PP,P}} + f_1^{\text{RR,P}} + f_1^{\text{PP,R}} + f_1^{\text{RR,R}} \tag{10.8.12}$$

where for example

$$\begin{aligned}
 f_1^{\text{RR,P}} &= \frac{1}{s} G_{\text{PP,P}}^{\text{RR,P}}(t) \left(\frac{s}{s_0}\right)^{2\alpha_R(t)} \left(\frac{M^2}{s_0}\right)^{\alpha_P(0)-2\alpha_R(t)} \\
 &\approx \frac{1}{s_0} G_{\text{PP,P}}^{\text{RR,P}}(t) \left(\frac{s}{M^2}\right)^{2\alpha'_R t} \tag{10.8.13}
 \end{aligned}$$

The terms in (10.8.12) all have $i = j$. There could also be cross terms like $f^{\text{PR,P}}$ which are usually neglected.

Clearly, by taking different types of particle for $\mathbf{3}$ one can examine a wide range of quantum numbers for $i = \overline{13}$: charge exchange, strangeness exchange, baryon exchange, etc. So far, only a limited amount of data is available but some fits have been made (e.g. Hoyer, Roberts and Roy 1973, Hoyer 1974).

Though the method is only directly applicable for $s > 100 \text{ GeV}^2$ we can extend it to lower values using duality arguments. Thus at low M^2 we can expect resonances (r) to be produced which will be dual to α_k ($k = R$) in the $i2 \rightarrow j2$ amplitude (fig. 10.23(c)). So we expect for $i = j$ in (10.8.6)

$$\left\langle \frac{d\sigma}{dt} \right\rangle^r \sim \left(\frac{M^2}{s_0} \right)^{\alpha_R(0) - 2\alpha_i(t)} \sim (M^2)^{(\alpha_R^0 - 2\alpha_i^0)} e^{-2\alpha_i t \log(M^2/s_0)} \tag{10.8.14}$$

for linear trajectories. This tells us how the differential cross-section in the two-body process $1 + 2 \rightarrow 3 + X$ should vary with M_X^2 at fixed s : it should broaden in t as M^2 increases. An example of how this occurs is shown in fig. 10.24. So the triple-Regge behaviour constrains quasi-two-body scattering as well.

In the triple-Regge fits to $pp \rightarrow pX$ it is always found that, for small t , $G^{PP,P}(t) \ll G^{RR,P}(t)$ but both are non-zero for $t = 0$ (see for example fig. 10.25). The precise value depends on the assumptions made about the secondary terms, but there is now fairly general agreement about this result (cf. Field and Fox 1974, Roy and Roberts 1974, Capella 1973, Lee-Franzini 1973). Since $\gamma_{pp}^P(t)$ is known from fits to the pp differential cross-section this gives $\gamma^{PP,P}(t, 0)$ directly (see (10.8.6)). Then if at a given fixed value of t we take out the factors $\gamma_{pp}^P(t)$, $\xi_P(t)$ and $(s/M^2)^{\alpha_P(t)}$, corresponding to the couplings and propagators of the Reggeons i, j in fig. 10.23(b), the remainder gives (from (10.8.5) and the optical theorem (1.9.6))

$$\sigma_{pp}^{tot}(M^2, t) \rightarrow \sum_k \gamma_{22}^k(0) \gamma^{PP,k}(t, 0) \left(\frac{M^2}{s_0} \right)^{\alpha_k(0) - 1}, \quad k = P, R, \dots \tag{10.8.15}$$

(where we have taken s_0/M^2 as the flux factor) which is the total cross-section for Pomeron-proton scattering as a function of the 'energy', M , and the (mass)² of the Pomeron, t . This is plotted in fig. 10.26 from which we see that at large M^2 $\sigma_{pp}^{tot} \rightarrow 1 \text{ mb}$ for $t \rightarrow 0$. Compared with $\sigma_{pp}^{tot} \simeq 40 \text{ mb}$ this shows that the triple-Pomeron coupling $\gamma^{PP,P}(0, 0) \approx \frac{1}{40} \gamma_{pp}^P(0)$, so Pomerons couple much more weakly to themselves than they do to other particles. But the coupling is not zero.

This raises a rather difficult point about the self-consistency of P exchange. The diffractive cross-section for $1 + 2 \rightarrow 3 + X$ (fig. 10.23(a))

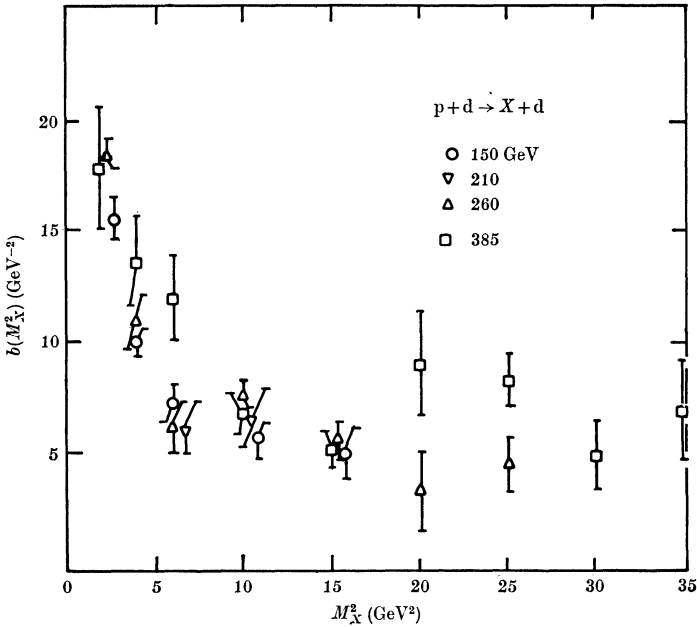


FIG. 10.24 The slope parameter b in $d^2\sigma/dt dM^2 \propto e^{b(M^2)t}$ as a function of M^2 in $p + d \rightarrow X + d$, from Loebinger (1974).

with $i = P$) is, from (10.8.6),

$$\frac{d^2\sigma}{dt dM^2} = \frac{G_{13,2}^{PP,P}(t)}{16\pi^2 s_0^2} \left(\frac{s}{s_0}\right)^{2\alpha_P(t)-2} \left(\frac{M^2}{s_0}\right)^{\alpha_P(0)-2\alpha_P(t)} \tag{10.8.16}$$

So if we put $\alpha_P(t) = \alpha_P^0 + \alpha'_P t$ the total diffractive contribution is given by

$$\sigma_{12}^D(s) = \frac{s^{2\alpha_P^0-2}}{16\pi^2 (s_0)^{\alpha_P^0}} \int_{\epsilon}^s \frac{dM^2}{(M^2)^{\alpha_P^0}} \int_{-\infty}^0 dt G_{13,2}^{PP,P}(t) e^{2\alpha_P' t \log(s/M^2)} \tag{10.8.17}$$

The boundary $M^2 = s$ is where $x = 1$, and ϵ marks the lower limit below which the triple-Regge approximation breaks down. Then putting say $G_{13,2}^{PP,P}(t) = G e^{at}$ for simplicity (see fig. 10.25)

$$\begin{aligned} \sigma_{12}^D(s) &= \frac{G s^{2\alpha_P^0-2}}{16\pi^2 (s_0)^{\alpha_P^0}} \int_{\epsilon}^s \frac{dM^2}{(M^2)^{\alpha_P^0} (a + 2\alpha'_P \log(s/M^2))} \\ &\sim s^{2\alpha_P^0-2} \end{aligned} \tag{10.8.18}$$

if $\alpha_P^0 < 1$. But if $\alpha_P^0 = 1$, using

$$\int \frac{dx}{x \log x} = \log(\log x), \tag{10.8.19}$$

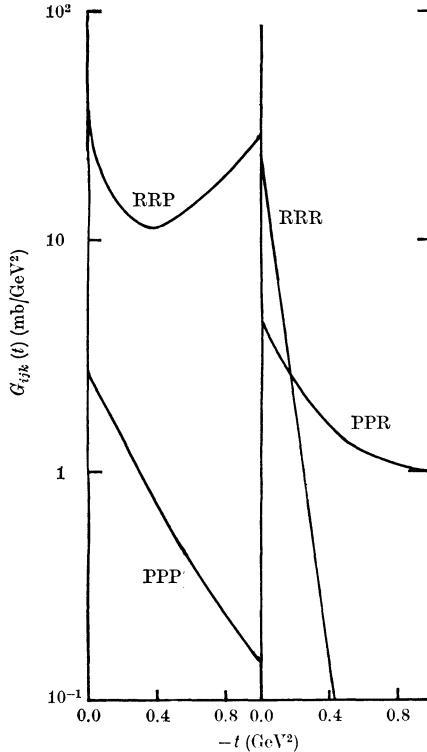


FIG. 10.25 The various triple-Regge couplings, $G^{i,j,k}$, found by Field and Fox (1974) in a fit to the $pp \rightarrow pX$ data.

we find
$$\sigma_{12}^D(s) \propto \frac{1}{2\alpha'_P} \log \left(1 + \frac{2\alpha'_P}{a} \log s \right) \sim \log(\log s) \quad (10.8.20)$$

Though this behaviour is compatible with the Froissart bound (2.4.10) there is evidently an inconsistency because $\alpha_P^0 = 1$ gives

$$\sigma_{12}^{\text{tot}}(s) \rightarrow \text{constant} - O((\log s)^{-1})$$

(see (8.6.9)) and clearly we must have $\sigma_{12}^D(s) < \sigma_{12}^{\text{tot}}(s)$ as $s \rightarrow \infty$. Indeed no ordinary Regge singularity can give $\sigma^{\text{tot}} \sim \log(\log s)$. On the other hand if $G_{13,2}^{\text{PP},P}(t)$ vanished at $t = 0$, for example

$$G_{13,2}^{\text{PP},P}(t) = (-t) G e^{at}$$

say, then (10.8.17) would give

$$\begin{aligned} \sigma^D \propto \int_{\epsilon}^s \frac{dM^2}{(M^2)^{\alpha_P^0} (a + 2\alpha'_P \log(s/M^2))^2} &\propto \frac{1}{2\alpha'_P a} - \frac{1}{2\alpha'_P (a + 2\alpha'_P \log s)} \\ \rightarrow \text{constant} - O((\log s)^{-1}) & \quad (10.8.21) \end{aligned}$$

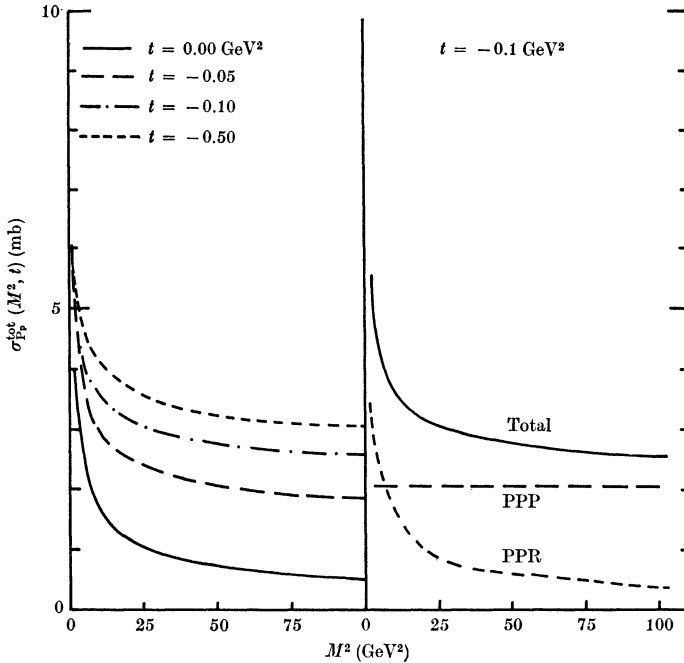


FIG. 10.26 The Pomeron-proton total cross-section $\sigma_{\text{Pp}}^{\text{tot}}(M^2, t)$ defined in (10.8.15) as a function of M^2 for various t , from Field and Fox (1974).

which would be compatible with P dominance. This problem, first noted in the context of the multi-peripheral model (see section 11.4 below) by Finkelstein and Kajantie (1968*a, b*), has been re-examined by many authors, for example Arbanel *et al.* (1971), Goddard and White (1972), Arbarbanel and Bronzan (1974*a*). A useful review of these arguments has been given by Brower and Weis (1975). Thus even though $\gamma^{\text{PP},\text{P}}(t)$ is small, the fact that empirically it appears to be non-zero at $t = 0$ raises an important difficulty which we shall examine further in the next chapter.

10.9 Finite-mass sum rules

In combining a Regge exchange model for the fragmentation region with Mueller's theorem in fig. 10.23 we have been led to study the discontinuity in M^2 of the Reggeon-particle scattering amplitude $A(i2 \rightarrow j2)$. From this viewpoint the function of particles 1 and 3 is simply to produce the virtual Reggeons, i, j . This is very analogous to

the way in which virtual photon amplitudes are produced in electro-production (cf. fig. 12.1 below).

The centre-of-mass energy for this Reggeon-particle amplitude is just M , the missing mass in $1 + 2 \rightarrow 3 + X$, and since to maintain the limit $s/M^2 \rightarrow \infty$ it is frequently necessary to consider rather small M^2 data it is useful to be able to obtain information about the Regge singularities, α_k , by using FESR to average over the resonance region of M^2 , in analogy with section 7.2, rather than trying to make Regge fits at high M^2 . These sum rules are called 'finite-mass sum rules', FMSR (see Hoyer 1974).

We begin by introducing the crossing-symmetric variable (cf. (7.2.3))

$$\nu \equiv p_2 \cdot (p_1 - p_3) \tag{10.9.1}$$

and, since

$$s \equiv (p_1 + p_2)^2 = m_1^2 + m_2^2 + 2p_1 \cdot p_2, \quad u \equiv (p_2 - p_3)^2 = m_2^2 + m_3^2 - 2p_2 \cdot p_3 \tag{10.9.2}$$

this can be rewritten, using (10.2.12), as

$$\nu = \frac{1}{2}(M^2 - t - m_2^2) \rightarrow \frac{1}{2}M^2 \quad \text{for} \quad M^2 \gg t, m_2^2 \tag{10.9.3}$$

Then from (10.8.6), taking just the leading $1\bar{3}$ trajectory $i = j$,

$$\frac{d^2\sigma}{dt dM^2} = \frac{1}{16\pi^2 s^2} |\gamma_{13}^i(t)|^2 |\xi_i(t)|^2 \left(\frac{s}{M^2}\right)^{2\alpha_i(t)} \times \text{Disc}_{M^2}\{A(i2 \rightarrow i2; t, M^2, 0)\} \tag{10.9.4}$$

and with (10.8.5) for $\text{Disc}_{M^2}\{A(i2 \rightarrow i2)\}$ we obtain, for an even-signature trajectory $\mathcal{S}_k = +1$ (cf. (7.2.8), (7.2.15)),

$$\int_0^N \nu d\nu \left(\frac{d^2\sigma(12 \rightarrow 3X)}{dt dM^2} + \frac{d^2\sigma(32 \rightarrow 1X)}{dt dM^2} \right) = \sum_k \frac{G_{13,2}^{ii,k}(t)}{16\pi^2 (s_0)^{\alpha_k(0)}} s^{2\alpha_i(t)-2} 2 \int_0^N (M^2)^{\alpha_k(0)-2\alpha_i(t)} \frac{1}{4} M^2 dM^2 \tag{10.9.5}$$

The factor 2 appears on the right-hand side because, as in (7.2.9), we are adding the cuts for positive M^2 and for negative M^2 , which describe the processes $12 \rightarrow 3X$ and $32 \rightarrow 1X$ respectively, at fixed $t_{22'} = 0$. These are the two discontinuities of the even-signature k trajectory (see fig. 10.27). And on performing the integration we obtain for the right-hand side

$$\sum_k \frac{G_{13,2}^{ii,k}(t) s^{2\alpha_i(t)-2}}{16\pi^2 (s_0)^{\alpha_k(0)}} \frac{1}{2} \frac{N^{\alpha_k(0)-2\alpha_i(t)+2}}{\alpha_k(0) - 2\alpha_i(t) + 2} \tag{10.9.6}$$

In practice it is not usually possible to go to sufficiently high energies

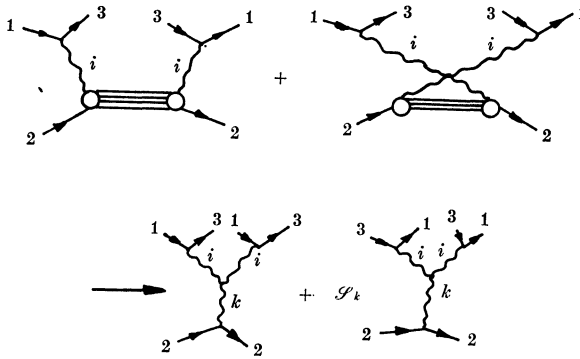


FIG. 10.27 Triple-Regge representations for $1 + 2 \rightarrow 3 + X$ and $3 + 2 \rightarrow 1 + X$ used for FMSR evaluations.

for a single trajectory i to contribute, and so it is necessary to replace \sum_k by $\sum_{i,j,k}$ in (10.9.6). Also we can take higher moments (like (7.2.14) and (7.2.16)) and obtain (setting $s_0 \equiv 1$ for convenience)

$$\int_0^N \nu^n d\nu \left[\frac{d^2\sigma(12 \rightarrow 3X)}{dt dM^2} + (-1)^{n+1} \frac{d^2\sigma(32 \rightarrow 1X)}{dt dM^2} \right] = \sum_{i,j,k} \frac{G_{13,2}^{ij,k}(t)}{32\pi^2} s^{\alpha_i(t)+\alpha_j(t)-2} \frac{N^{\alpha_k(0)-\alpha_i(t)-\alpha_j(t)+n+1}}{\alpha_k(0) - \alpha_i(t) - \alpha_j(t) + n + 1} \quad (10.9.7)$$

where $n = 1, 3, 5, \dots$, for $\mathcal{S}_k = 1$ and $n = 0, 2, 4, \dots$ for $\mathcal{S}_k = -1$.

These FMSR were introduced by Einhorn *et al.* (1972a) and Sanda (1972) and have been widely employed to complement triple-Regge fits. For example Roy and Roberts (1974) and Field and Fox (1974) used them in the fits described in the previous section.

The duality properties of these sum rules are rather interesting. For $i, j = R$ (i.e. ordinary Reggeons, not P) we can expect the usual two-component duality of two-body reactions (section 7.3), i.e. resonances in M^2 will be dual to $k = R$, while the non-resonant background should be dual to $k = P$, since all we have done is move out in t along the i, j trajectories away from the physical particles. This seems to be well verified (see Hoyer 1974). But what about the Pomeron-particle amplitude $P + 2 \rightarrow P + 2$? On the basis of the duality diagrams, fig. 10.28 (a), (b), Einhorn *et al.* (1972) argued that (unlike $R + 2 \rightarrow R + 2$) the resonances in M^2 build up the P exchange. But on the other hand if the P couples through the f, the resonances should be dual to the R and P is dual to the background as in fig. 10.28 (c).

However, this diagram contains a closed loop and so would normally be excluded from consideration. The 'theory' is thus ambiguous, and so unfortunately is the phenomenology at present (see Hoyer 1974).

By taking wrong-moment sum rules (i.e. n even for $\mathcal{S}_k = +1$, and n odd for $\mathcal{S}_k = -1$) we can explore the fixed poles which may be present in the Reggeon-particle scattering amplitudes (cf. (7.2.21)). For example if in an even-signature amplitude we take the zeroth moment we obtain (with $j = i$, and again setting $s_0 = 1$)

$$\begin{aligned} \int_0^N d\nu \left(\frac{d^2\sigma(12 \rightarrow 3X)}{dt dM^2} + \frac{d^2\sigma(32 \rightarrow 1X)}{dt dM^2} \right) \\ = \sum_{i,k} \frac{1}{16\pi^2 s^2} |\gamma_{13}^i(t)|^2 |\xi_i(t)|^2 s^{2\alpha_i(t)} \gamma_{22}^k(0) \\ \times \frac{1}{2} \left[G_1^{ii}(t) + \gamma^{ii,k}(t, 0) \frac{N^{\alpha_k(0) - 2\alpha_i(t) + 1}}{\alpha_k(0) - 2\alpha_i(t) + 1} \right] \end{aligned} \quad (10.9.8)$$

where $G_m^{ii}(t)$ are the residues of the fixed poles in the Reggeon-particle amplitude $i2 \rightarrow i2$ at the nonsense points $J - 2\alpha_i(t) = -m$, $m = 1, 3, 5, \dots$ (since the t -channel helicities of the trajectories are $\alpha_i(t)$). $G_1^{ii}(t)$ is related to the Reggeon-particle fixed-pole coupling $N_1(t, t_1, t_2)$ which occurs in the expressions (8.2.37) and (8.3.8) for a Regge cut in the Gribov calculus by (see (8.2.39))

$$G_1^{ii}(t) = N_1^{ii}(0, t, t) (\gamma_{22}^i)^{-1} \quad (10.9.9)$$

Thus by comparing right- and wrong-moment sum rules one can in principle evaluate N and substitute it into (8.4.1) and obtain an expression for the Regge cut. This has been attempted by Roberts and Roy (1972) who used inclusive data on $K^+ \rightarrow K^0$ and $K^- \rightarrow \bar{K}^0$ to evaluate $\rho \otimes \rho$ and $A_2 \otimes A_2$ cuts in $pp \rightarrow pp$, and by Muzinich *et al.* (1972) who have tried to estimate the $P \otimes P$ cut in $pp \rightarrow pp$. They find that the cut has a strength of only about 40 per cent of the eikonal/absorption prescription ($N_1^{PP}(t, t_1, t_2) = 1$, see section 8.4). However, the uncertainties in the triple-Reggeon couplings make the errors in these evaluations rather large. Also the procedure is not self-consistent since the cuts have been omitted from the inclusive sum rules, so this approach can only be even approximately successful if cuts \ll poles.

It will be evident from the preceding sections that, despite being restricted to $t_{22} = 0$, this triple-Regge regime should eventually provide many useful insights into Reggeon dynamics.

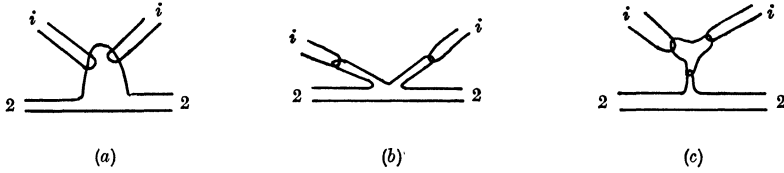


Fig. 10.28 (a) Duality diagram for P exchange in $i2 \rightarrow i2$. (b) A redrawing of (a) suggesting that the P-exchange coupling might be dual to the resonances. (c) An alternative duality diagram, involving a closed loop, which suggests that P exchange is dual to the background as usual.

10.10 Correlations and the correlation length

The two-particle inclusive distribution for $1 + 2 \rightarrow 3 + 4 + X$ was defined in (10.3.12). The dynamics of particle production can obviously be explored further by observing any correlations there may be between the two observed final-state particles. For example if 3 and 4 were mainly produced through a resonance decay, $1 + 2 \rightarrow r + X$, $r \rightarrow 3 + 4$, then the momenta of these particles would be closely related.

We can define the two-particle correlation function by

$$c_2(\mathbf{P}_3, \mathbf{P}_4, s) \equiv \rho_2(\mathbf{P}_3, \mathbf{P}_4, s) - \rho_1(\mathbf{P}_3, s)\rho_1(\mathbf{P}_4, s) \quad (10.10.1)$$

where the ρ 's are defined in (10.3.10) and (10.3.15). If there is no correlation between the production of particles 3 and 4 the probability of producing both must be just the product of the individual production probabilities, i.e.

$$\rho_2(\mathbf{P}_3, \mathbf{P}_4, s) = \rho_1(\mathbf{P}_3, s)\rho_1(\mathbf{P}_4, s) \quad (10.10.2)$$

giving $c_2 = 0$ as required. It is also convenient to introduce

$$C_2(s) \equiv \int c_2(\mathbf{P}_3, \mathbf{P}_4, s) \frac{d^3\mathbf{P}_3}{16\pi^2 E_3} \frac{d^3\mathbf{P}_4}{16\pi^2 E_4} = \langle n_3 n_4 - \delta_{34} n_3 \rangle - \langle n_3 \rangle \langle n_4 \rangle \quad (10.10.3)$$

from (10.10.1), (10.3.16) and (10.3.11). If 3 and 4 are identical particles

$$C_2(s) = F_2(s) - F_1^2(s) \quad (10.10.4)$$

We have seen in fig. 10.5 that $F_1 \sim \log s$ approximately, and similarly (fig. 10.29) $C_2(s) \sim (\log s)^2$ approximately (or it could be \sim a small power of s).

Likewise we can define the three-particle correlation by

$$c_3(\mathbf{P}_3, \mathbf{P}_4, \mathbf{P}_5, s) = \rho_3(\mathbf{P}_3, \mathbf{P}_4, \mathbf{P}_5, s) - \rho_1(\mathbf{P}_3, s)c_2(\mathbf{P}_4, \mathbf{P}_5, s) - \rho_1(\mathbf{P}_4, s) \times c_2(\mathbf{P}_3, \mathbf{P}_5, s) - \rho_1(\mathbf{P}_5, s)c_2(\mathbf{P}_3, \mathbf{P}_4, s) - \rho_1(\mathbf{P}_3, s)\rho_1(\mathbf{P}_4, s)\rho_1(\mathbf{P}_5, s) \quad (10.10.5)$$

and so on.

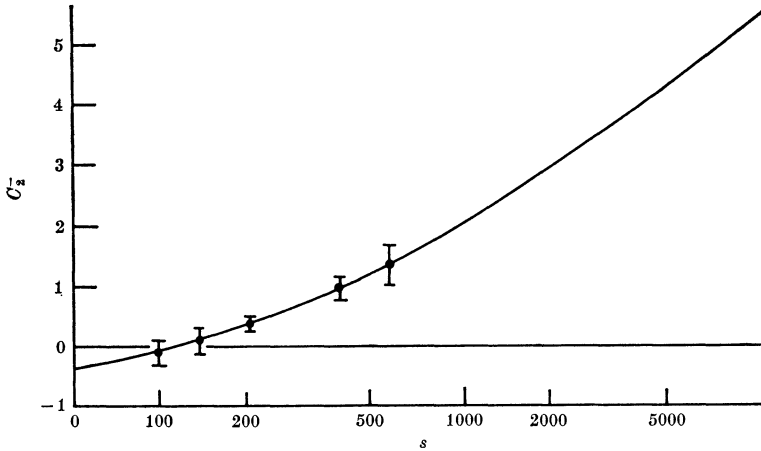


FIG. 10.29 Data on $C_2(s)$ against s for negatively charged particles, from Harari (1974). The curve is a fit with $C_2^- = 0.14(\log s)^2 - 0.65 \log s + 0.06$.

Some correlations have to be present because of kinematics (i.e. conservation of E , \mathbf{p} , etc.), or quantum number conservation (of B , Q , S , I , G etc.): see de Tar, Freedman and Veneziano (1971). For example, since in $1 + 2 \rightarrow 3 + 4 \dots (m + 2)$ we have

$$\sum_{n=3}^{m+2} E_n = \sqrt{s} \quad (10.10.6)$$

i.e. the total centre-of-mass energy of all the outgoing particles must equal that of the initial state, and there is an energy conservation sum rule

$$\sum_l \int E_l \rho_l(\mathbf{p}_l, s) \frac{d^3 \mathbf{p}_l}{16\pi^2 E_l} = \sqrt{s} \quad (10.10.7)$$

since the left-hand side gives the probability of producing a particle of type l with energy E_l , integrated over all possible energies, and summed over all possible types of particles. Also since

$$\left(\sum_{n=3}^{m+2} E_n \right)^2 = s \quad (10.10.8)$$

we have similarly

$$\sum_{\substack{k, l \\ k \neq l}} \int E_k E_l \rho_2(\mathbf{p}_k, \mathbf{p}_l, s) \frac{d^3 \mathbf{p}_k}{16\pi^2 E_k} \frac{d^3 \mathbf{p}_l}{16\pi^2 E_l} + \sum_l \int E_l^2 \rho_1(\mathbf{p}_l, s) \frac{d^3 \mathbf{p}_l}{16\pi^2 E_l} = s \quad (10.10.9)$$

But since from (10.10.1) we can express ρ_2 in terms of c_2 and ρ_1 , and

since
$$\sum_{\substack{k,l \\ k \neq l}} E_k E_l \rho_1(\mathbf{p}_k, s) \rho_1(\mathbf{p}_l, s) \frac{d^3 \mathbf{p}_k}{16\pi^2 E_k} \frac{d^3 \mathbf{p}_l}{16\pi^2 E_l} = s \quad (10.10.10)$$

we obtain from (10.10.9)

$$\sum_{\substack{k,l \\ k \neq l}} \int E_k E_l c_2(\mathbf{p}_k, \mathbf{p}_l, s) \frac{d^3 \mathbf{p}_k}{16\pi^2 E_k} \frac{d^3 \mathbf{p}_l}{16\pi^2 E_l} + \sum_l \int E_l^2 \rho_1(\mathbf{p}_l, s) \frac{d^3 \mathbf{p}_l}{16\pi^2 E_l} = 0 \quad (10.10.11)$$

The second term is clearly positive definite, and so c_2 must be negative. Obviously one would expect to obtain a negative correlation from any conserved quantity like energy, because the larger the energy carried by particle 3, the more likely it is that the energy of 4 will be small. Similarly from charge conservation we have (like (10.10.7))

$$\sum_l \int Q_l \rho_1(\mathbf{p}_l, s) \frac{d^3 \mathbf{p}_l}{16\pi^3 E_l} = \sum_l Q_l \langle n_l \rangle = Q_1 + Q_2 \quad (10.10.12)$$

using (10.3.11), which gives a negative correlation between the charges of the particles produced in a reaction.

In addition to these kinematic correlations there may be dynamical correlations due to the production mechanism, for example the resonance decay mentioned above. Such correlations seem much less likely if the particles occur at very widely spaced points on the rapidity plot (fig. 10.4), and it is useful to try and determine the distance in rapidity over which one can expect there to be strong correlations. This is called the ‘correlation length’, Λ , defined such that there will be negligible correlation between particles 3 and 4 if

$$|y_3 - y_4| \gg \Lambda \quad (10.10.13)$$

Thus the projectile fragmentation region of fig. 10.4 (b) is

$$y_{3 \max} \geq y_3 > (y_{3 \max} - \Lambda) = \frac{1}{2} \log (s/\mu_3^2) - \Lambda$$

and the target fragmentation region is

$$y_{3 \min} \leq y_3 < (y_{3 \min} + \Lambda) = -\frac{1}{2} \log (s/\mu_3^2) + \Lambda.$$

Note that since we are taking Λ to be independent of s we are assuming that scaling holds in the central region. But for low s , $\Lambda > \log (s/\mu_3^2)$, so the two fragmentation regions overlap and scaling is not expected.

In the central region the Mueller–Regge diagram for

$$1 + 2 \rightarrow 3 + 4 + X$$

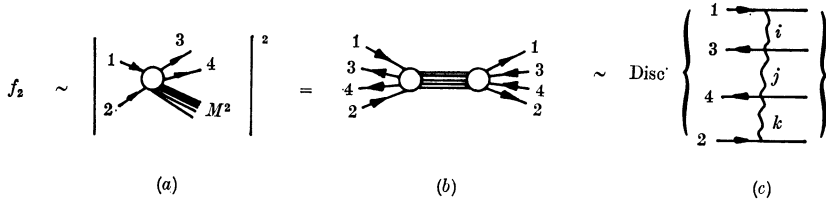


FIG. 10.30 Treble-Regge representation of the two-particle inclusive process $1 + 2 \rightarrow 3 + 4 + X$.

is the treble-Regge diagram fig. 10.30, where $s_{12}, t_{13}, s_{34}, t_{24} \rightarrow \infty$ with $(t_{13} s_{34} t_{24})/s_{12}$ etc. fixed. And so (cf. (10.6.4))

$$f_2(\mathbf{P}_3, \mathbf{P}_4, s) \rightarrow \sum_{i,j,k} \gamma_{ijk}(\mu_3^2, \mu_4^2) \left| \frac{t_{13}}{s_0} \right|^{\alpha_j(0)-1} \left| \frac{t_{34}}{s_0} \right|^{\alpha_j(0)-1} \left| \frac{t_{42}}{s_0} \right|^{\alpha_k(0)-1} \tag{10.10.14}$$

Once the energy is high enough for the central region to be really well separated from the fragmentation regions, we need only include the P for i and k , so for $t_{13}, t_{24} \rightarrow \infty$, if $\alpha_P(0) = 1$,

$$f_2(\mathbf{P}_3, \mathbf{P}_4, s) \rightarrow \sum \gamma_{PjP}(\mu_3^2, \mu_4^2) \left(\frac{s_{34}}{s_0} \right)^{\alpha_j(0)-1} \xrightarrow{s_{34} \rightarrow \infty} \gamma_{PPP}(\mu_3^2, \mu_4^2) \tag{10.10.15}$$

which gives the scaling behaviour expected in the central region. How fast the latter limit is approached depends on the spacing of the secondary trajectories, R, in the sum over j .

Using factorization we can write (cf. (10.6.6))

$$\gamma_{PjP}(\mu_3^2, \mu_4^2) = \gamma_{11}^P \gamma_{33}^{Pj}(\mu_3^2) \gamma_{44}^{jP}(\mu_4^2) \gamma_{22}^P \tag{10.10.16}$$

So using (10.5.7) we can write, from (10.3.15) and (10.10.15),

$$\rho_2(\mathbf{P}_3, \mathbf{P}_4, s) \rightarrow \gamma_{33}^{PP}(\mu_3^2) \gamma_{44}^{PP}(\mu_4^2) \tag{10.10.17}$$

which is independent of the nature of particles 1 and 2. Then because of (10.6.7) we find

$$\rho_2(\mathbf{P}, \mathbf{P}_4, s) \rightarrow \rho_1(\mathbf{P}_3, s) \rho_1(\mathbf{P}_4, s) \tag{10.10.18}$$

and so from (10.10.1) $c_2(\mathbf{P}_3, \mathbf{P}_4, s) \rightarrow 0$ and there is no correlation. This is because we have assumed that asymptotically a single factorizable pole dominates, and so each vertex is completely independent.

However, at lower s_{34} we can expect corrections to the Regge behaviour from the lower-lying R trajectories, and these will produce correlations between the particles at non-asymptotic sub-energies.

To determine the length in rapidity over which such correlations will occur we note that in terms of rapidity, from (10.2.18),

$$p_3 = (\mu_3 \cosh y_3, \mathbf{P}_{3T}, \mu_3 \sinh y_3)$$

$$p_4 = (\mu_4 \cosh y_4, \mathbf{P}_{4T}, \mu_4 \sinh y_4)$$

and so

$$s_{34} \equiv (p_3 + p_4)^2 = p_3^2 + p_4^2 + 2p_3 \cdot p_4$$

$$= m_3^2 + m_4^2 + 2\mu_3\mu_4 \cosh y_3 \cosh y_4 - 2\mathbf{P}_{3T} \cdot \mathbf{P}_{4T}$$

$$\quad - 2\mu_3\mu_4 \sinh y_3 \sinh y_4$$

$$= m_3^2 + m_4^2 + 2\mu_3\mu_4 \cosh (y_3 - y_4) - 2\mathbf{P}_{3T} \cdot \mathbf{P}_{4T}$$

$$\xrightarrow{s_{34} \rightarrow \infty} 2\mu_3\mu_4 \cosh (y_3 - y_4) \rightarrow \mu_3\mu_4 e^{|y_3 - y_4|} \tag{10.10.19}$$

Hence (10.10.15) gives

$$f_2(\mathbf{P}_3, \mathbf{P}_4, s) \rightarrow \sum_j \gamma_{PjP} (\mu_3^2, \mu_4^2) \left(\frac{\mu_3\mu_4}{s_0} \right)^{\alpha_j(0)-1} e^{(\alpha_j(0)-1)|y_3 - y_4|} \tag{10.10.20}$$

The first term with $j = P$, $\alpha_P(0) = 1$, gives no correlation as we have seen, but the second term with $j = R$, $\alpha_R(0) \approx 0.5$, gives a contribution

$$\rho_2(\mathbf{P}_3, \mathbf{P}_4, s) \propto e^{-\frac{1}{2}|y_3 - y_4|} \tag{10.10.21}$$

which in (10.10.1) gives

$$c_2(\mathbf{P}_3, \mathbf{P}_4, s) \propto e^{-\frac{1}{2}|y_3 - y_4|} \tag{10.10.22}$$

and so if we define the correlation length λ as the distance in rapidity within which the correlation has fallen to e^{-1} of its maximum value, then Regge theory predicts that

$$\lambda = (\alpha_P(0) - \alpha_R(0))^{-1} = 2 \tag{10.10.23}$$

This seems to be quite well verified in many processes. See for example fig. 10.31 which shows how the events peak in a ridge where $y_3 \approx y_4$. This number is quite important as it gives the width in rapidity of the fragmentation regions, and shows that we need $Y \approx 8$ (as at the CERN-ISR) before the central region is well separated from them.

This prediction depends crucially on the fact that each Regge pole contribution must factorize, so that only the non-factorizability of a sum of Regge poles produces correlations. However, Regge cut contributions will in general not factorize, and so for example $P \otimes P$ cuts could produce correlations of infinite correlation length. The apparent absence of very strong long-range correlations must mean

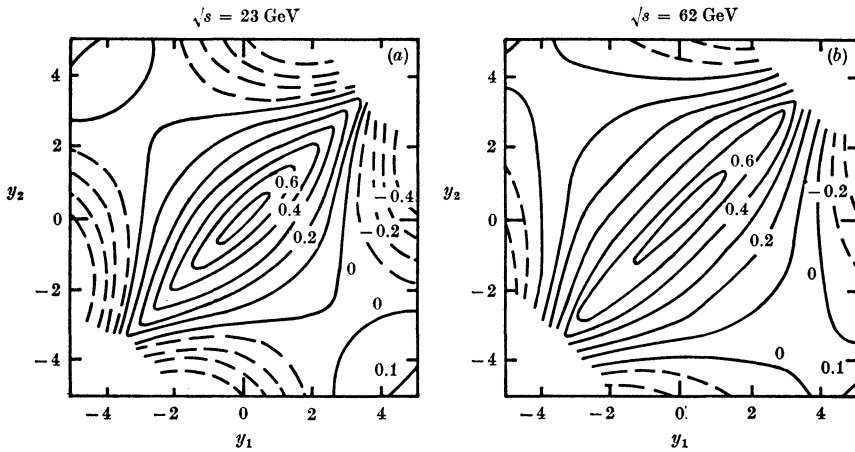


FIG. 10.31 Contours of constant correlation $c_2(y_3, y_4; s)$, in the y_3 - y_4 plane, for charged particle pairs (mainly pions) produced in pp collisions at CERN-ISR, from Zalewski (1974).

that the P singularity is at least approximately factorizable, and lends support to the view that it is effectively a pole at available energies. However, we shall see in the next chapter that there are some long-range correlation effects.